DESIGN AND ANALYSIS OF ULTRA-WIDE BANDWIDTH IMPULSE RADIO RECEIVER

by

Sangyoub Lee

A Dissertation Presented to the

FACULTY OF THE GRADUATE SCHOOL

UNIVERSITY OF SOUTHERN CALIFORNIA

In Partial Fulfillment of the

Requirements for the Degree

DOCTOR OF PHILOSOPHY

(ELECTRICAL ENGINEERING)

August 2002

Dedication

To My Family and Friends .....

Acknowledgements

I would like to thank the many friends and colleagues who have supported and challenged me during my graduate study at University of Southern California. Fist and foremost, I wish to acknowledge my advisor Professor Robert Scholts who gave me great opportunity to join UWB research, and Professor John Choma Jr. for his valuable technical advisements. Also I like to give my great appreciation to Professor Richard E. Kaplan from the department of Aerospace and Mechanical Engineering, Professor Hans H. Kuehl and Professor Martin A. Gundersen who served on my committee and whose thoughtful comments also improved the final manuscript of this work.

I would also like to thank Professor Namgoong who took time for valuable discussion out of his very busy schedule. I am also grateful for my officemate Pansop, and uncle Jun Huh who spare time for me to discuss. Also, I wish to thank all the member of UWB group especially Joonyong and Eric who helped my research.

Anther group of people that I must be grateful for are the CSI staffs: Milly, Mayumi, and Gerrielyn. They contribute disproportionately to making CSI a wonderful place. Their assistance and professionalism in the area of administrative support was essential part of my study.

In addition to those community, I'd like to thank Army Research Office and National Science foundation for grants during my UWB research. Also, I wish to thank EE-system and EE-Physics both departments for the continuing teaching assistantship. Especially I wish to thank Mona in EE-Physics for her help.

Finally, I must reserve the most special thanks for my friends and family, who have been enriched my life in many ways. I thank my friends at USC and elsewhere for their support and friendship. Among those that I have not already mentioned are my undergraduate seniors at USC: Jong-Soong, Kyongsu, and Woohyun. Also, I wish to thank my friends in Korea. I am deeply indebted to my family for their unconditional support. My parents, brother and sister have always been there for me throughout the whole stage of my study and the hardships that they have to endure. It would be impossible that I could ever repay what they have done to me but I hope that my humble accomplishment can compensate for what little part of their efforts and sacrifices.

Contents

List Of Tables

List Of Figures

Abstract

The wireless system is being rapidly proliferated in our life. The growing of capacity in wireless communication requires a new type of wireless communication method which does not effect current systems. A new system that fulfills this requirement is the Ultra-Wide bandwidth (UWB) impulse radio. In addition, the UWB system also promises low power, covert communication, and very high processing gain. In this dissertation, an UWB system which can lead this next generation of communications of an UWB radio is introduced.

In this work, the complete front-end of an UWB radio and its components are described in a detailed analysis. The main focus of this work is the design of the UWB system's wide-bandwidth components.

In the course of this dissertation, the UWB system, its UWB signal properties and its possible system architecture are described. Based on these system characteristics, required RF components are designed with IBM's Silicon Germanium (SiGe) 0.5 μm process and analyzed. Using this technology, the two important front-end functions highlighted in this work are signal amplification for wide-bandwidth and correlation detection of the signal.

Theoretical investigation of the conventional front-end components illustrates deficiencies of current technologies that frustrate the wide-bandwidth design task. Along with these investigations, possible solutions for wide-bandwidth components design are provided.

As final goals of this dissertation, the new UWB system design has been constructed with a sinusoidal correlator template, and a wide-bandwidth LNA and mixer have been designed. The LNA achieves 0.8 GHz bandwidth, 8.4 dB flat gain over its frequency range, 3 dB noise figure and -6 dBm dynamic range with shunt-series feedback topology. The mixer achieves 13 dB conversion gain, 15 dB noise figure and -6.3 dB dynamic range using the CS-CG pair as the mixer's transconductance.

Chapter 1

Introductions

During the last decade, communication technology has undergone rapid commercial development for wireless applications. In addition, the advanced signal processing and very large scale integrated circuit (VLSI) technology have accelerated wireless communication implementation.

1.1 Motivation

Every communication system designer worth his salt would be pleased to have more data modulation bandwidth by a factor of 10 or 100 than he has now because more radio frequency (RF) bandwidth promises a higher data transmission rate. Work on circuits and systems that can operate on gigahertz wide signals will undoubtedly be the wave of the future as pressures to supply multimedia services over wireless continue to build.

The popularity of cellular telephones and pagers has led many manufacturers to enter the wireless market[5]. Currently high-data-rate wireless digital communication is an important component of the market. New applications are being allocated high-frequency bands. However with current narrow-band technology, high frequency signals can not satisfy the demands for high transmission data rate, secure communication, and better material penetration. Therefore, a new technology for these demands will be necessary, namely Ultra Wide Bandwidth radio (UWB).

In most high-frequency communication system, Gallium-Arsenide(GaAs) metal-semiconductor-field-effect transistor (MESFET) and heterojunction bipolar transistor (HBT) show their strong presence in RF product because they give high performance on output power [26][19]. However with GaAs technology, it is difficult to expect high yield and to achieve a integrated solution such as the system on the chip(SOC) [47] because the cost of the process[9]. Therefore many less expensive, high performance technologies have been challenging for RF IC circuit.

Silicon germanium (SiGe) technology has been reported as having inherently higher linearity and lower phase noise, and SiGe devices are stable over a wider range of temperature than other existing technologies. The key advantage of SiGe is its compatibility with mainstream CMOS processing. This provides a huge economic benefit because mature CMOS is the IC industry cost leader. Another advantage of SiGe process is that it provides a high frequency capability on the identical silicon platform where digital processing functions can also be integrated. Considering the trend in RF and mixed signal applications is toward an integrated solution, this technology is suitable for UWB system design.

In this work, a low noise amplifier (LNA), and a mixer for the wide-bandwidth system will be presented. These components are designed with IBM 0.5 μm SiGe technology and will demonstrate the possibility of hardware implementation of the UWB radio. These two components of UWB system have most important roll as a correlator that is detect an UWB signal.

1.2 Overview

The following chapters delve into the problem of UWB radio design from its basic communication concept to circuit design and analysis. The ultimate goal for this work is to design the front-end of UWB radio in 0.5 μm SiGe process.

Chapter 2 begins with an overview of RF circuit design fundamentals. Also an overview of basic UWB radio architecture is presented and the UWB signal format is introduced. This UWB signal format provides important parameters of the UWB component design. In chapter 3, a new UWB system will be introduced with its analytical background. The next chapters explores hardware implementations. Chapter 4 introduces the wide-bandwidth LNA utilizing current LNA topologies. The designed LNA will be introduced and analyzed. Chapter 5 will describe a new design of the mixer. This chapter also starts with background on a mixer design. A few different type of mixers will be introduced and their strengths and weaknesses are discussed. Then the schematic of a new mixer will be explained in detail. This chapter concludes with a specification of the characteristics of this new mixer. Finally the last chapter contains a summary and some suggestions for future work.

Chapter 2

RF Fundamentals and Basic of Ultra-Wide Bandwidth Radio

The goal of this chapter is to provide a formal review of the basic concepts of radio frequency (RF) circuits and a description of an ultra-wide bandwidth (UWB) signal. The design of the UWB system and its components requires a strong background in these topics. Hence, the following sections give essential knowledge of RF systems and the UWB signals.

2.1 RF System Fundamentals

In any RF system, the matching, noise, and linearity are the basic specifications of system performance. Impedance matching is the major contributor to gain efficiency. The noise characteristic affects to the system sensitivity. Linearity limits the system's working range. In this section, these important considerations of RF system design are described.

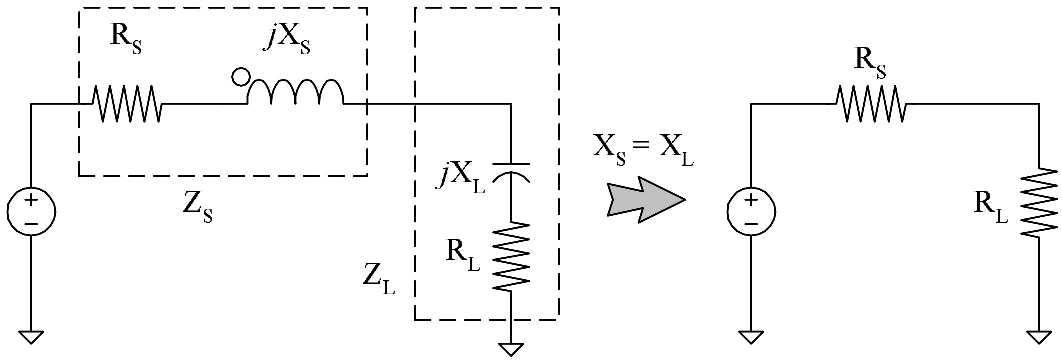

Figure 2.1: Impedance driving its complex conjugate and its equivalent circuit

2.1.1 Impedance Matching

To achieve maximum power transfer, impedance matching between the load and the source is the essential requirement. Usually this matching is accomplished by passive networks connected between the source and the load. These matching networks works not only are designed to achieve minimum power loss between the load and the source, but also are based on minimizing noise influence, maximize power handling capability and linearizing the frequency response.

The basic idea of the matching comes from the well known theorem which states that, for DC circuits, maximum power will be transferred from the source to the load if the load resistance equals the source resistance. However in the case of AC or time-varying wave forms, this theorem states that the maximum power transfer occurs when the load impedance is equal to the *complex conjugate* of the source impedance. If the source impedance is described, by $Z_S = R + jX$, then the load impedance should be $Z_L = R - jX$, its complex conjugate. Therefore as shown in the figure 2.1, the inductive and capacitive reactance compensate for each other and an equivalent real impedance is the result.

Simple real impedance matching is very rare in the real world. Most devices, e.g., transistor, transmission lines, LNAs, mixers, antenna systems, etc., source and load impedances are almost always *complex* because devices contain some reactive components. Therefore it is very important to know how to handle these reactive components. There are two different ways to handle these. One is the analytical method and the other is the graphical method using the Smith chart. The first approach yields very precise results but is complicated. The second approach is more intuitive, easier, and fast because it does not require complicated computation.

In the analytical method, the quality factor analysis (Q analysis) is the most common way to construct the matching network. The basic definition of the quality factor of a circuit is

$$Q = \omega \frac{\text{energy stored}}{\text{average power dissipated}}. \tag{2.1}$$

The figure 2.2 is the simple matching network which is known as an $L - match$ because its shape. In this figure, from the definition of Q, the serial network Q_s and the parallel network Q_p can be described as

$$Q_s = \frac{X_s}{R_s}, \tag{2.2}$$

$$Q_p = \frac{R_p}{X_p}. \tag{2.3}$$

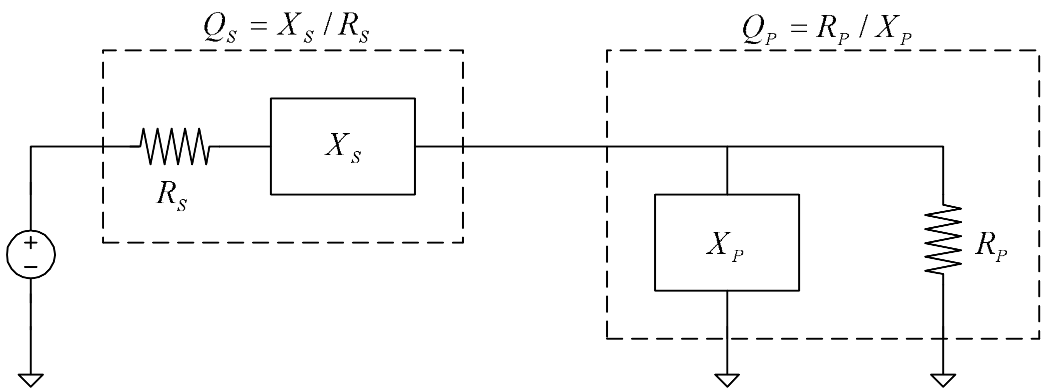

Figure 2.2: Simple L-matching network

To match the source and the load, $R_s + jX_s$ and $R_p \parallel jX_p$ should be same. Therefore,

$$\begin{aligned} R_s + jX_s &= \frac{jX_pR_p}{R_p + jX_p} \\ &= \frac{jX_pR_p^2 + X_p^2R_p}{R_p^2 + X_p^2}. \end{aligned} \tag{2.4}$$

If we equate the real parts of the equation 2.4 and use equation 2.3,

$$\begin{aligned} R_s &= \frac{X_p^2R_p}{R_p^2 + X_p^2} \\ &= \frac{R_p}{Q_p^2 + 1}. \end{aligned} \tag{2.5}$$

From equation 2.5, the Q_p can be described with resistive components only.

$$Q_p = \sqrt{\frac{R_p}{R_s} - 1}. \tag{2.6}$$

If we consider the Q_p and the Q_s must be same to construct matching network, X_p and the X_s can be calculated from equations 2.2, 2.3 and 2.6.

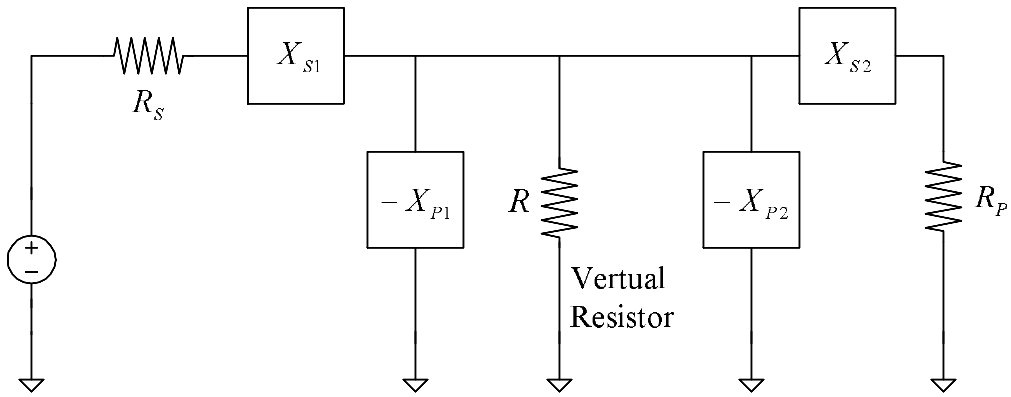

Figure 2.3: The T-matching network as a combination of L-matching network

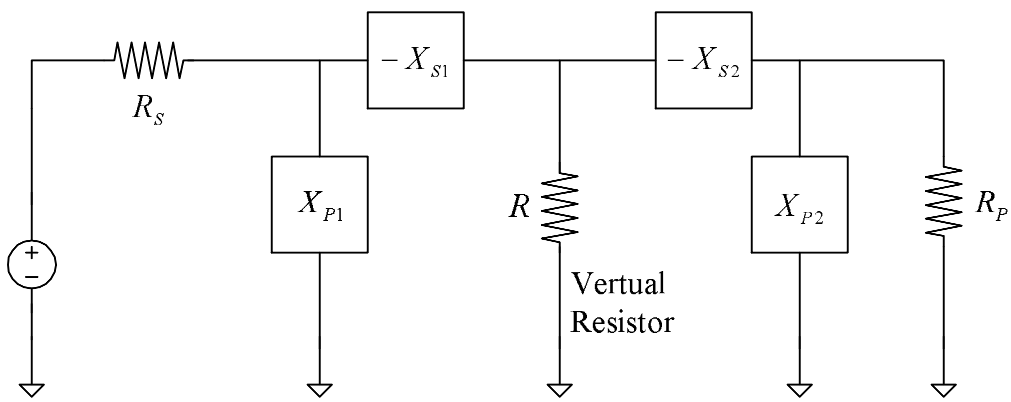

Figure 2.4: The pi-matching network as a combination of L-matching network

This analytical method can be applied to other basic matching networks such as $\pi - match$ and $T - match$ because these basic matching networks can be described as combinations of $L - match$ network as shown in figure 2.3 and 2.4. The analytical method for matching these networks requires a complex calculation even though the matching network is relatively simple. A simple way to make the matching network is uses a Smith chart as a useful graphical tool to find the correct matching network easily. The Smith chart is the simple circular form deriving from mapping the resistance lines and reactance lines in the impedance plane ($Z - plane$) into the plane of reflection coefficients ($\Gamma - plane$). Since the $\Gamma - plane$ represents the presentation of the reflection coefficient Γ in real and imaginary coordinates, the reflection coefficient should be described.

The reflection coefficient is defined as the ratio of reflected voltage wave to incident voltage wave at the input from a source to a load. Given a source impedance, the reflection coefficient Γ of a load impedance can be found by

$$\Gamma = \frac{Z_s - Z_L}{Z_s + Z_L}. \tag{2.7}$$

In normalized form,

$$\Gamma = \frac{Z_0 - 1}{Z_0 + 1}, \tag{2.8}$$

where Z_0 is a complex impedance of the form $R + jX$. The polar form of reflection coefficient can be described in rectangular coordinates as

$$\Gamma = \Gamma_r + j\Gamma_i. \tag{2.9}$$

Therefore from equations 2.8 and 2.9, the real and imaginary part of reflection coefficients can be found as

$$\Gamma_r = \frac{R^2 - 1 + X^2}{(R+1)^2 + X^2}, \tag{2.10}$$

$$\Gamma_i = \frac{2X}{(R+1)^2 + X^2}. \tag{2.11}$$

The reactance X can be eliminated by combining equation 2.10 and 2.11.

$$\left(\Gamma_r - \frac{R}{R+1}\right)^2 + \Gamma_i^2 = \left(\frac{1}{R+1}\right)^2 \tag{2.12}$$

Similarly, the resistance R also can be eliminated to give

$$(\Gamma_r - 1)^2 + \left(\Gamma_i - \frac{1}{X}\right)^2 = \left(\frac{1}{X}\right)^2. \tag{2.13}$$

The Smith chart can be constructed from these two circular equations 2.12 and 2.13.

The figure 2.5 shows how to construct matching network using the Smith chart[24]. This example shows how the matching circuit can be constructed between the source impedance $Z_S = (50+j25)\Omega$ and the load impedance $Z_L = (25-j50)\Omega$ using the Smith chart. In most RF circuits, the characteristic impedance of $Z_0 = 50\Omega$ is a standard. Using this, the normalized load and source impedances Z_S and Z_L are

$$z_S = \frac{Z_S}{Z_0} = 1 + j0.5, \tag{2.14}$$

$$z_L = \frac{Z_L}{Z_0} = 0.5 - j, \tag{2.15}$$

then plot the z_S and z_L^* on the Smith chart. In this case, four possible configurations of $L - match$ networks are expected. For example, if the path $z_S \rightarrow z_C \rightarrow z_L^*$ is chosen, the $L - match$ network between the source and load constructed with a series capacitance and a shunt inductance. As summary, the additional reactance

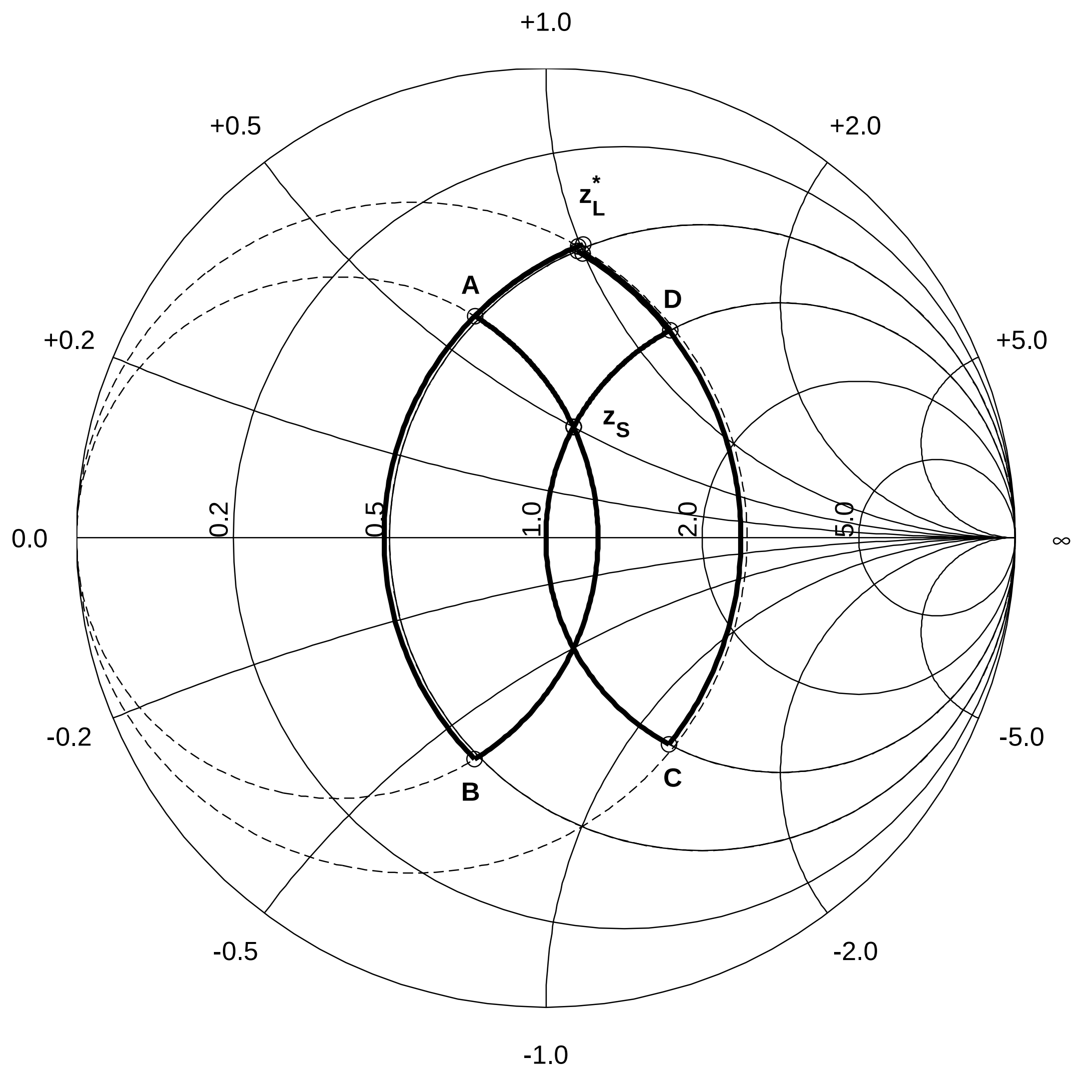

Figure 2.5: Example of matching network construction using the Smith chart

connected in series with a complex impedance results in motion along a constant resistance circle in the combined Smith chart. In contrast, a shunt connection produces motion along a constant conductance circle.

Furthermore, using a three-element matching network, it is easy to find the system's nodal quality factor Q_n.

2.1.2 MDS and Noise in Radio Receivers

The performance of a radio system can be characterized by its ability to detect a weak signal. This system performance can be denoted in terms of the minimum detectable signal (MDS) level at the antenna. To calculate the MDS, the noise characteristics of the receiver must be discussed. Noise can be defined as any undesired signal that interferes with the desired signal to be processed. There are several forms of electrical noise in circuits including thermal noise and shot noise. The noise behavior can be described with random variables of Gaussian distribution and zero mean. Although the mean of the noise is zero, the root mean square (RMS) value of noisy a voltage in the system can not be zero. Therefore the RMS noise voltage can be described as

$$V_{nRMS} = \sqrt{V_n^2} = \sqrt{\lim_{T_M \to \infty} \int_{T_1}^{T_1+T_M} [v_n(t)]^2 dt} \quad \neq \quad 0, \tag{2.16}$$

where T_1 is an arbitrary point in the time and T_M is the measurement interval.

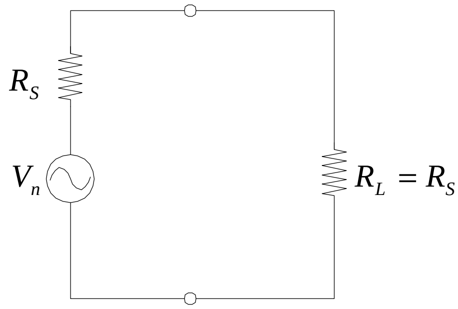

Figure 2.6: Noise voltage of a circuit

Current flow though a resistance generates noise due to the random motion of charge carriers in the conductor. Therefore the noise power in a conductor can be quantified as

$$P_n = kT\Delta f = kTB, \tag{2.17}$$

where k is Boltzmann's constant$(1.38 \times 10^{-12} J/^{\circ}K)$, T is absolute temperature in $^{\circ}K$ and $\Delta f = B$ is the noise bandwidth (Hertz) of the measurement system. This noise bandwidth is defined as a function of the instrument's gain $G(f)$.

$$B = \frac{1}{G_{max}} \int_0^{\infty} G(f) df, \tag{2.18}$$

where G_{max} is the maximum gain of the instrument. Suppose there is a noiseless resistance R_S connected to the noise voltage source and the load resistance R_L connected under matching condition (figure 2.6). Then the noise power of the load resistor is given as

$$P_n = \frac{V_{nRMS}^2}{4R_S} = kTB. \tag{2.19}$$

From equation 2.19, the RMS noise voltage is easily found. From this V_{nRMS}, the spectral density $S(f)$ is used to quantify the noise content in a unit bandwidth of 1 Hz. Therefore if $S(f)$ associated with resistor R, it can be denoted as,

$$S(f) = \frac{V_n^2}{B} = 4kTR. \tag{2.20}$$

If this $S(f)$ is constant over the frequency range of the system, it is called white noise.

The noise figure (NF) is commonly used as a figure of merit to compare the noise in a network. The IEEE definition of noise factor (F) is the ratio of available output noise power to available output noise power due to the source equated in 2.21.

$$F \triangleq \frac{\text{Total output noise power}}{\text{total output noise due to the source}} \tag{2.21}$$

When this noise factor is expressed as decibel, it is called as *noise figure*(NF). Also this noise figure can be defined as the ratio between the input SNR to the output SNR at the output port of a network, i.e. the degradation in SNR that a system introduced.

$$F = \frac{SNR_{in}}{SNR_{out}} \tag{2.22}$$

In two port system, the ratio of the signal to noise power at input and output port can be rewritten as

$$F = \frac{P_1/P_{n1}}{P_2/P_{n2}}. \tag{2.23}$$

Applying the available power gain of the system G_A, then P_2 andP_{n2} at the input become $G_A P_1$ and $G_A P_{n1} + P_{ni}$ respectively at the output.

$$F = 1 + \frac{P_{ni}}{G_A P_{n1}}, \tag{2.24}$$

where P_{ni} is the internally generated noise power within the amplifier. This noise factor also can be described in the power notation. Assuming the input impedance Z_{in} in the two port system is matched with source impedance Z_S, the noise factor can be denoted with the noise voltage and the noise current.

$$F = 1 + \frac{V_n^2 + (I_n Re\{Z_{in}\})^2}{4kTBRe\{Z_{in}\}}. \tag{2.25}$$

The noise power per unit frequency bandwidth can be calculated as P_n =-174 dbm/Hz at room temperature. so including the noise figure from 2.25, the minimum detectable signal (MDS) level can be described as

$$MDS = -174\text{dBm/Hz} + NF + 10\log BW + SNR_{min}, \tag{2.26}$$

where note that the sum of the first three terms is the total integrated noise of the system and is called the noise floor.

2.1.3 Signal Distortion and Dynamic Range

The signal distortion and the dynamic range are other important characteristics of a system. If noise of the radio receiver sets its sensitivity, then the signal distortion that is created by a system's nonlinearity sets the maximum signal level of the system. Although most of the system design uses a linear approximation, that model is not valid in its non-linear region. This signal distortion can be specified by *1 dB compression point*. As the input signal approaches to the system's saturation region, the system signal gain begins to fall off. The point where the gain of the system deviates from its linear approximation by 1 dB is called the 1 dB compression point. This 1 dB compression point can be used to be defined the extent of the linear region. Therefore the system's dynamic range can be defined as the power difference from the noise level to the 1 dB compression point. Figure 2.7 shows how the dynamic range is set from the relationship between input and output power.

Two other characteristics of a narrow bandwidth system are the intermodulation distortion (IMD) and the third order intercept point (IIP_3). These characteristics come from the result of applying two unmodulated sinusoidal signals of slightly different frequencies to the input of a system. When two signals with different frequencies are applied to a nonlinear system, the output exhibits some components

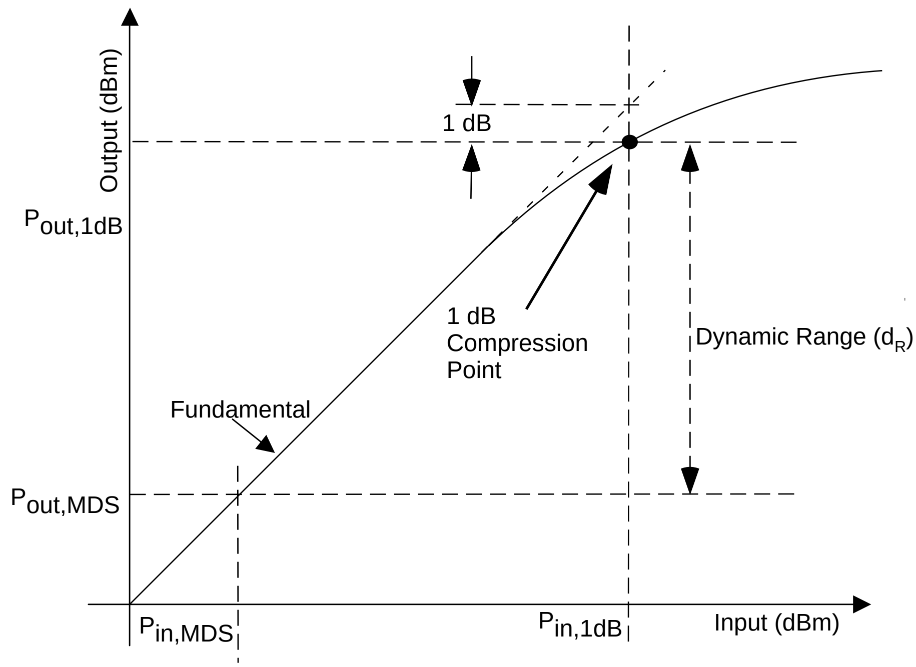

Figure 2.7: The dynamic range of a system from the input and output power relation

that are not harmonics of the input frequencies. Applying an input consisting of two closely-spaced sinusoidal components $V_{in} = A\cos(\omega_1 t) + A\cos(\omega_2 t)$, then the nonlinear system output comes as a power series $V_{out} = k_1 V_{in} + k_2 V_{in}^2 + k_3 V_{in}^3$ where k_1, k_2 and k_3 are gain. Expending this output, it contains several distortion products at frequencies $n\omega_1 \pm m\omega_2$ where $n + m$ is the order of the distortion product. The amplitude of each product varies as A^{n+m} so, second-order products vary in proportion to A^2 and third-order products in proportion to A^3. Note that in a differential implementation, the second-order distortion is cancelled. Thus the third-order intermodulation distortion merits special attention. Figure 2.8 illustrates the behavior of the third-order intermodulation products with input amplitude. With the input and output amplitudes plotted on a log scale, the intermodulation product amplitudes

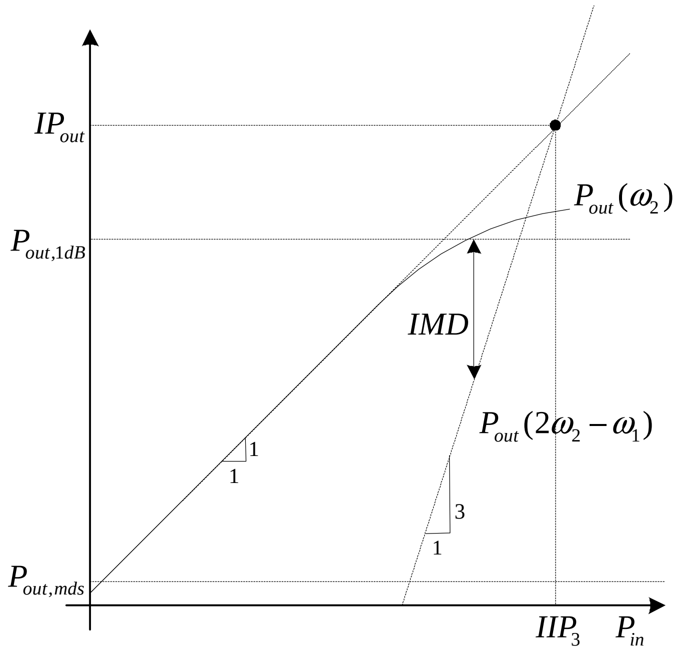

Figure 2.8: Intermodulation behavior based on input-output power relation.

follow straight line trajectories with slopes given by the order of the products. By extrapolating, intercept point can be found that serve as a characteristic for the linearity of a system.

In current communication systems, there are two different way to define a system's linearity. One is the dynamic range and the other is the IIP_3 as described above. Between these two definition, the dynamic range, which is defined by the 1 dB compression point is more general term for the linearity. Since the 1 dB compression point can be determined by the system's gain saturation, this definition can be used both the narrow bandwidth and the wide bandwidth system. Therefore the dynamic range is more important in a UWB system than the IIP_3.

2.2 UWB Signal Overview

A successful radio system design requires understanding of the characteristics of the signal which drives the system. Since this UWB radio is much different from conventional radio system, understanding of these signal characteristics is very important. In this section, the signal waveform, characteristics of the UWB system, and detection method will be discussed.

2.2.1 UWB Impulse Signal Characteristics

The UWB impulse radio transmits very short duration Gaussian monocycle pulses as a signal without a sinusoidal carrier. The very short duration of the monocycle naturally yields very wide bandwidth signals. According to the definition of the UWB signal[10] as shown in the equation 2.27, the bandwidth of the impulse radio signal is large enough to be qualified as a UWB signal.

$$\text{Fractional Bandwidth} = \frac{2(f_H - f_L)}{f_H + f_L} \geq 25\% \tag{2.27}$$

Figure 2.9 and figure 2.10 are show experimental measurements of a received monocycle waveform in the time and the frequency domain. As shown in these figures, when the monocycle's pulse width is about 1.2 ns, the frequency bandwidth is about 520 MHz with the center frequency of 1.12 GHz, which are completely dependent upon the pulse's width[44].

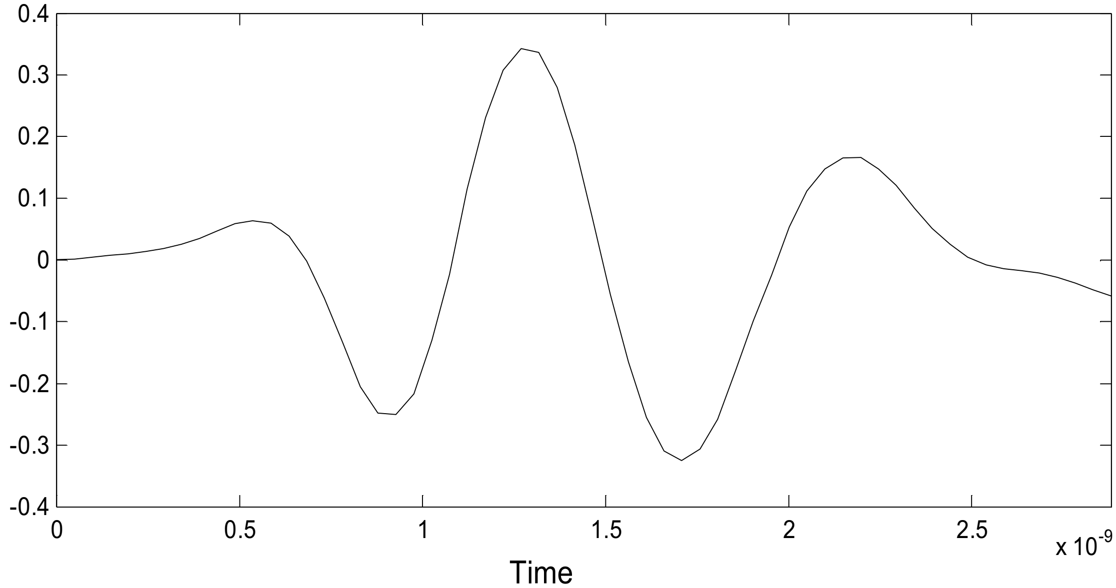

Figure 2.9: Received UWB signal in time domain

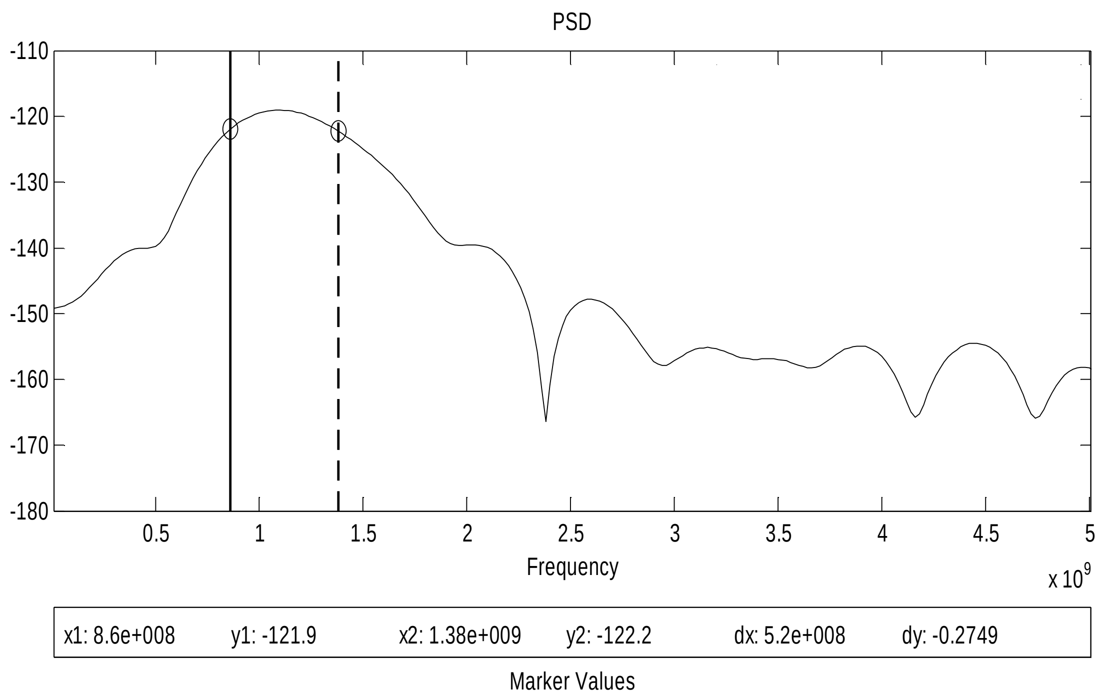

Figure 2.10: Received UWB signal in frequency domain

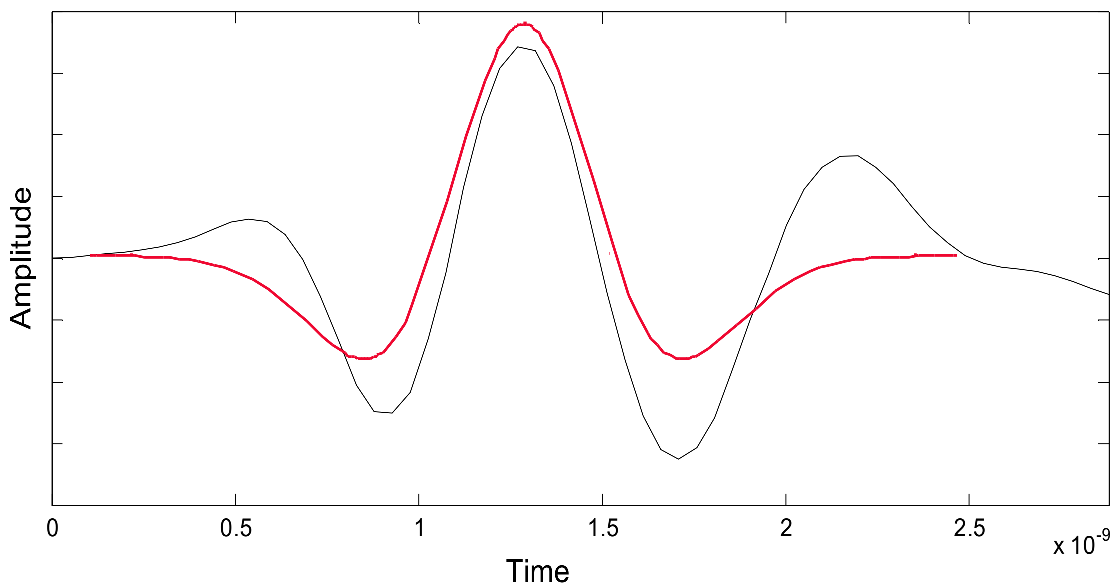

Figure 2.11: UWB pulse model overlapped with measured data

An often used model of a UWB signal can be described as the second derivative of a Gaussian function:

$$\omega(t) = \sqrt{\frac{4}{3\tau\sqrt{\pi}}}(1-(\frac{t}{\tau})^2)\exp(-\frac{1}{2}(\frac{t}{\tau})^2), \tag{2.28}$$

where the factor $\sqrt{\frac{4}{3\tau\sqrt{\pi}}}$ ensures that the received signal is normalized, therefore

$$\int_{-\infty}^{\infty} \omega^2(t)dt = 1 \tag{2.29}$$

The figure 2.11 is the pulse shape which generated from the equation 2.28.

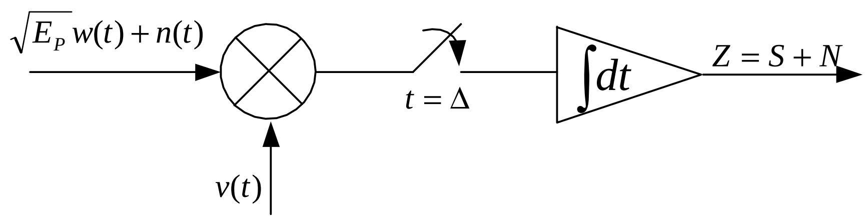

Figure 2.12: The correlator which is used in the UWB system

2.2.2 Signal to Noise Ratio Calculation

The basic system configuration of the UWB receiver is the correlator as shown in figure 2.12. Using the equation 2.28, the average output signal-to-noise ratio of the UWB radio can be calculated. The signal portion of the correlator output S is computed as

$$S = \sqrt{E_p}\int_{-\Delta}^{\Delta}\omega(t)v(t)dt, \tag{2.30}$$

where $\sqrt{E_p}$ is the amplitude of the incoming signal, $v(t)$ is the template signal and Δ is the correlation time. Considering a timing error τ_e which can exist between the input signal and the template signal, the cross-correlation function is defined as

$$R_{\omega v}(\tau_e) = \int_{-\Delta}^{\Delta}\omega(t)\cdot v(t-\tau_e)dt. \tag{2.31}$$

Therefore the signal component of the correlator output can be described as a function of timing error

$$S = \sqrt{E_p}R_{\omega v}(\tau_e). \tag{2.32}$$

The noise portion of the correlator output N is a random variable due to the white noise $n(t)$. The mean of the white noise $n(t)$ is zero while the auto-correlation function is $R_{nn}(t_1, t_2) = N_0\delta(t_1 - t_2)$. Note that the thermal noise process described in section 2.1.2 can be considered to be a white noise process over the operating band where $N_0 = kT$. Thermal noise also happens to have a Gaussian distribution[4]. Therefore the mean of N is zero and the variance is

$$\begin{aligned}
E(N^2) &= E\int_{-\Delta}^{\Delta}\int_{-\Delta}^{\Delta} n(t_1)n(t_2)v(t_1)v(t_2)dt_1dt_2 \\
&= \int_{-\Delta}^{\Delta}\int_{-\Delta}^{\Delta} E\{n(t_1)n(t_2)\}v(t_1)v(t_2)dt_1dt_2 \\
&= \int_{-\Delta}^{\Delta}\int_{-\Delta}^{\Delta} R_{nn}(t_1, t_2)v(t_1)v(t_2)dt_1dt_2 \\
&= N_0\int_{-\Delta}^{\Delta}\int_{-\Delta}^{\Delta} \delta(t_1 - t_2)v(t_1)v(t_2)dt_1dt_2 \\
&= N_0\int_{-\Delta}^{\Delta} v^2(t)dt \\
&= N_0R_{vv}(0), \qquad (2.33)
\end{aligned}$$

where the R_{vv} is the auto-correlation of the template signal $v(t)$.

$$R_{vv}(\tau_e) = \int_{-\Delta}^{\Delta} v(t)v(t - \tau_e)dt \qquad (2.34)$$

Therefore from the definition of the signal-to-noise ratio $S^2/E(N^2)$, the correlator output SNR is

$$SNR = \frac{E_p}{N_0}\frac{R^2_{\omega v}(\tau_e)}{R_{vv}(0)}. \qquad (2.35)$$

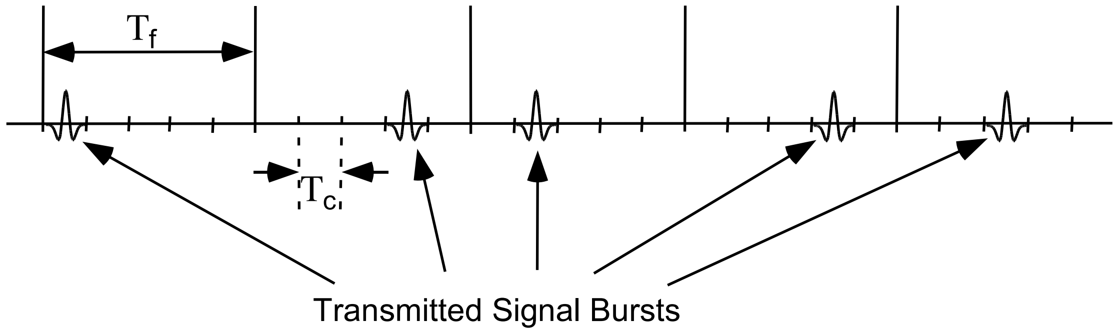

Figure 2.13: Time hopped pulse train with the sequence of 0,3,1,3,2.

2.2.3 Time Hopping format using the impulse

In the UWB system, long sequences of pulses are used with time-hopping (TH) pulse-position modulation for the communication. This TH modulation makes more uniform the distribution of the RF signal power over its frequency band. This effect causes the UWB signal to resemble noise in the frequency domain. Therefore the UWB signal is less detectable, and resistant to jamming from other communication systems.

Figure 2.13 shows a typical time-hopping signal controlled by the pseudo random (PN) sequence used in the UWB system. The transmitter bursts one monocycle in a time frame location determined by PN code sequence. This basic UWB signal form can be described[32, 43] as

$$s(t) = \sum_j \omega(t - jT_f - c_j T_c - d_{\lfloor j/N_{rep} \rfloor}) \tag{2.36}$$

where ω is the monocycle waveform. The frame time T_f is usually hundred times wider than the monocycle signal, resulting in a signal with a very low duty cycle.

The c_j represents a distinctive time-hopping sequence pattern, d represents the data sequence, which is addition binary pulse position modulation, and T_c is the duration of addressable time delay bins.

2.2.4 Processing Gain of UWB signal

Like most spread spectrum systems, processing gain is an important characteristic in a UWB system. The processing gain (PG) is defined as the ratio of the RF spread bandwidth to the bandwidth of the information signal at the receiver output. This PG can be described in dB for the direct sequence system as [23]

$$PG = 10 \cdot \log(\frac{T_s}{T_c}) \tag{2.37}$$

where T_s is the symbol time and T_c is the chip time. This PG can be applied to UWB system. Since in the UWB system, only one signal bursts in one frame, the PG for the UWB system can be defined as

$$PG = 10 \cdot \log(\frac{T_f}{T_c}) + 10 \cdot \log(N_{rep}) \tag{2.38}$$

where T_f is the frame time and N_{rep} is the number of repetitions of the monocycle signal in one symbol time. Suppose the frame time (T_f) is 1 μs and the chip time (T_c) is 1 ns as described previous section. With the first term of the equation 2.38, the PG for the UWB radio will be about 30 dB. However, this value comes only from its duty cycle. Since the UWB uses multiple pulses to recover each bit of information, there will be another 20 dB gain added if the energy integration is made over 100 pulses to determine one digital bit. Therefore the total PG for the UWB radio is about 50 dB with 1 μs frame time and 100 repetition of the signal and a 1 ns pulse, and the resulting data rate is 10 Kbps. This 50 dB of PG is a large amount of gain compared with many other communication systems.

Chapter 3

Ultra-Wide Bandwidth Receiver Architecture

In this chapter, the UWB receiver architecture will be discussed focussing on correlator template generation. The basic building block of this receiver is the correlator. Therefore the template which is correlated with the incoming signal is very important. The sinusoidal template for this receiver is compared with the ideal template in the following chapter. In addition to this, the synchronization method with this sinusoidal template will be described.

3.1 Template of the Correlation Detector

Usually the UWB receiver is analyzed a second derivative Gaussian model correlator template as its local reference signal. However this second derivative Gaussian template signal is difficult to generate in the circuits. Since the input signal of the UWB receiver is the same as one and a half cycles of a sinusoidal wave, the sinusoidal wave is a candidate for the template. Current system designs use a rectangular gate on the central peak of the received signal as a template.

3.1.1 Ideal Template for UWB Radio

To compare the sinusoidal template with the second derivative Gaussian model, the correlated signal characteristics with the second derivative Gaussian template will be discussed first. Assume that the second derivative Gaussian template signal $v(t)$ is exactly same shape with incoming signal $\omega(t)$, i.e., $v(t) = \omega(t)$, then the correlator output SNR is

$$SNR = \frac{E_p}{N_0} \frac{R^2_{\omega v}(\tau_e)}{R_{vv}(0)}. \tag{3.1}$$

When the timing error τ_e is zero, the maximum output SNR can be obtained as

$$SNR_{MAX} = \frac{E_p}{N_0} R_{vv}(0). \tag{3.2}$$

In this case, the maximum output SNR can be found when the correlation function $R(0)$ is maximum with the optimum value of the correlation time. Figure 3.1 shows the output correlation function which related with the correlation time. As shown in this figure 3.1, if the correlation is performed over a large enough time interval, then the maximum SNR E_p/N_0 can be achieved. In more general case, i.e., the timing error τ_e is not zero, the SNR will be degraded. The output SNR normalized by E_p/N_0 is plotted in the figure 3.2.

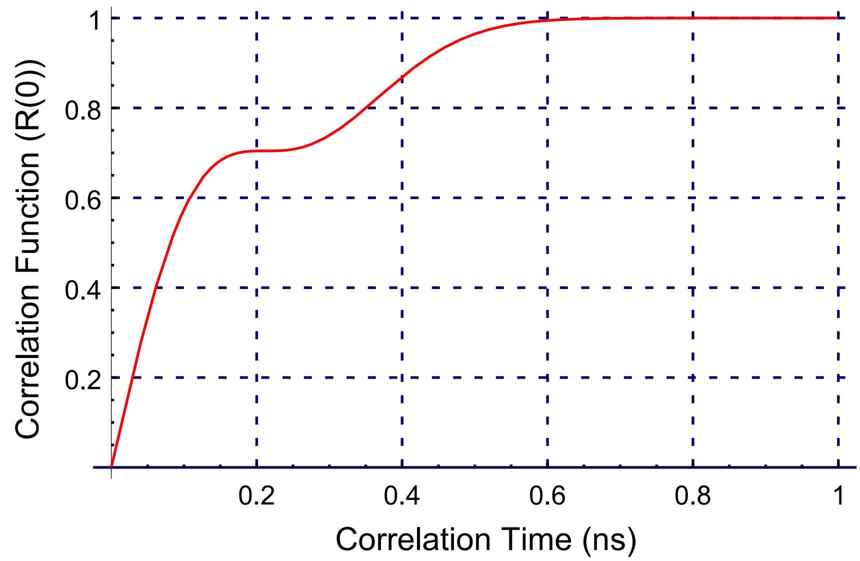

Figure 3.1: The relation of the correlation function R_0 and the correlation time

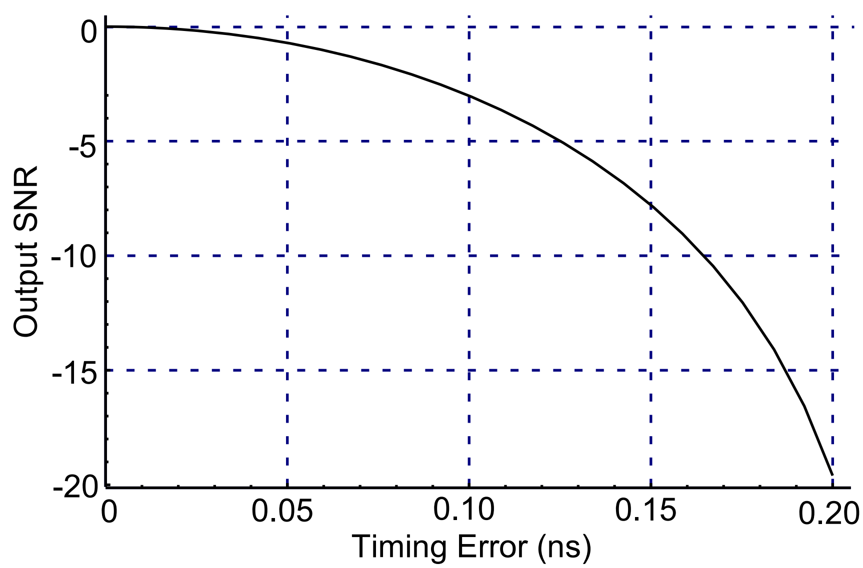

Figure 3.2: Output SNR degradation (dB) when the timing error become larger.

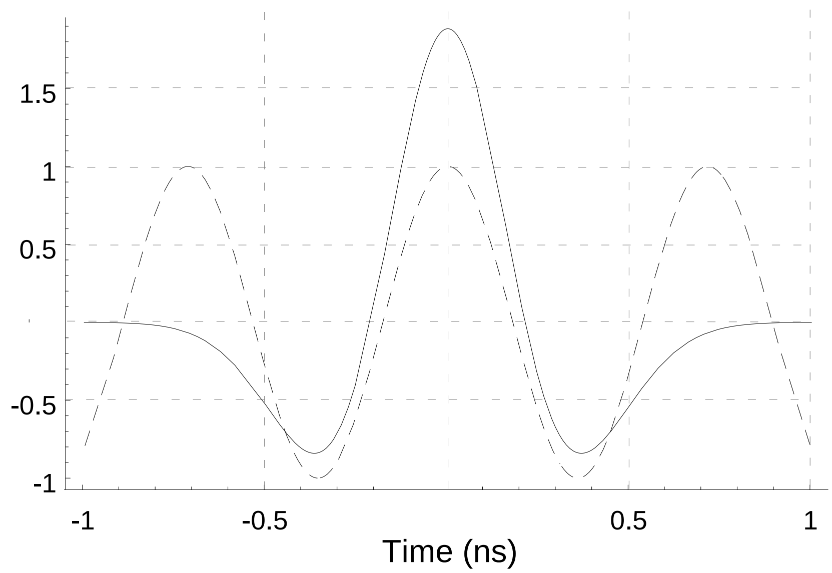

Figure 3.3: Sinusoidal template overlapped with the second derivative Gaussian model template.

3.1.2 Sinusoidal Template for UWB Radio

The simpler suboptimal sinusoidal template signal, $v(t) = \cos(2\pi f_c t)$, is examined and compared with the second derivative Gaussian model template. Figure 3.3 and 3.4 show the properly aligned oscillator sinusoidal template with specific oscillator frequency f_c. This oscillator frequency should be chosen so as to maximize the output SNR of the correlator. To find out this aligned oscillator frequency, the maximum output SNR is calculated from 3.3.

$$SNR = \frac{E_p}{N_0} \frac{(\int_{-\Delta}^{\Delta} \omega(t) \cos(2\pi f_c(t - \tau_e))dt)^2}{\int_{-\Delta}^{\Delta} \cos^2(2\pi f_c t)dt} \tag{3.3}$$

Therefore the output SNR becomes the function of two variables, timing error (τ_e) and the alignment frequency (f_c). In addition to this variables, the correlation time

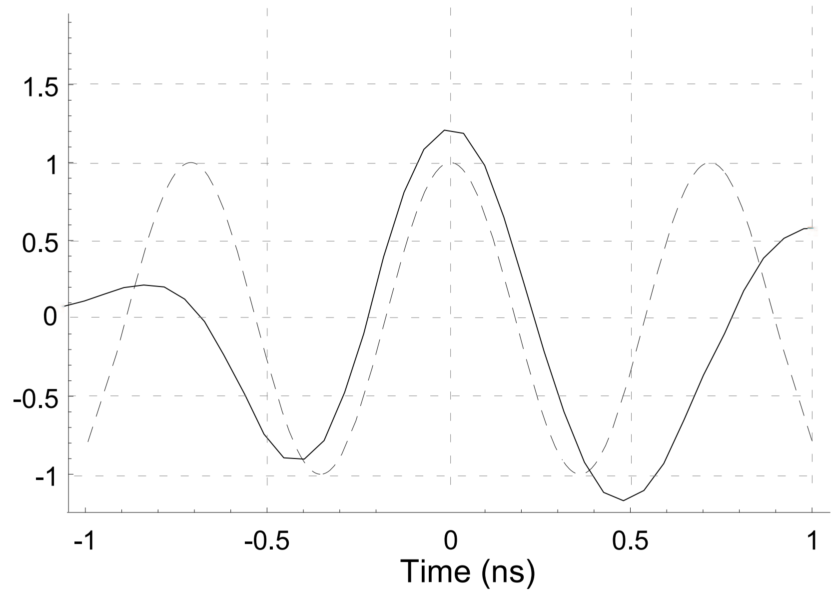

Figure 3.4: Sinusoidal template overlapped with the incoming UWB signal.

becomes important factor in the sinusoidal template. If there is no timing error, as shown in the figure 3.5, the maximum SNR can be plotted as a function of the alignment frequency and the correlation time. Since the sinusoidal template is continuous through the time line, the maximum correlation value is appear at the certain time period.

To find out the usefulness and robustness of the sinusoidal template, SNR degradation is good measure. The degradation to output SNR with respect to the second derivative Gaussian model template's maximum achievable SNR is E_p/N_0 divided by the sinusoidal template output SNR. Therefore the the degradation of the sinusoidal template output SNR as a function of τ_e and f_c is

$$Degradation = \frac{\int_{-\Delta}^{\Delta} \cos^2(2\pi f_c t) dt}{(\int_{-\Delta}^{\Delta} \omega(t) \cos(2\pi f_c(t - \tau_e)) dt)^2}. \tag{3.4}$$

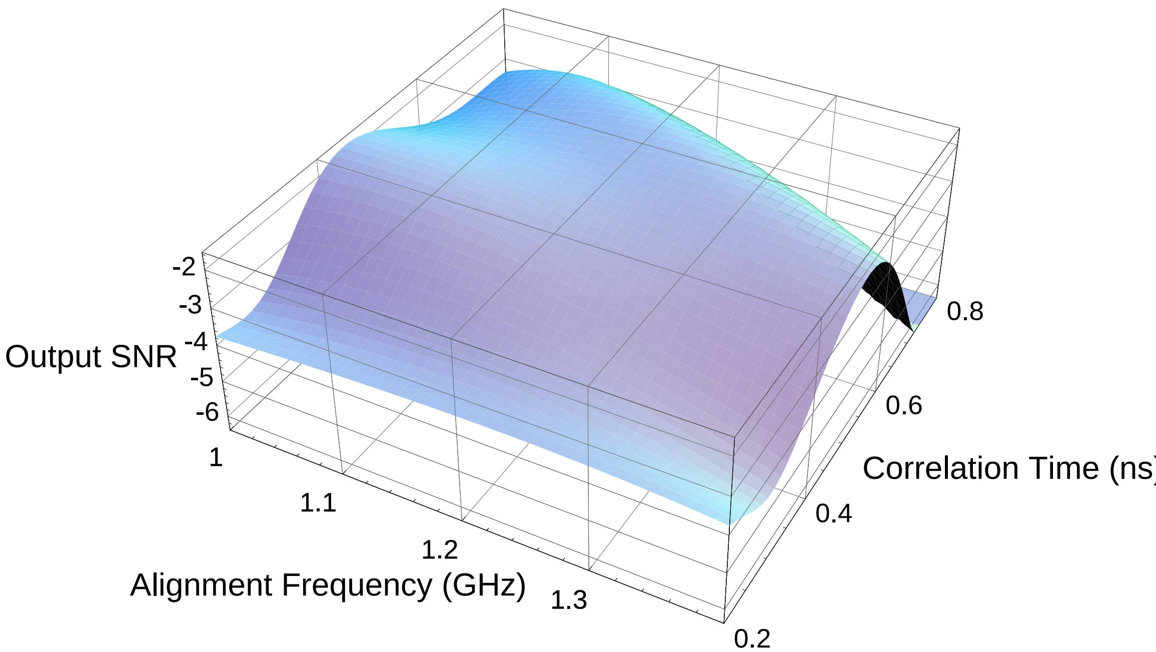

Figure 3.5: The output SNR with the sinusoidal template when the alignment frequency and correlation time shift.

Figure 3.6 shows the output SNR degradation versus template frequency f_c for different values of correlation time τ_e. As shown in this figure, the lowest degradation is roughly 1.7 dB when the frequency of 1.25 GHz and the correlation time $\Delta = 0.6$ ns. In this this figure, one noticeable phenomenon is when the correlation time is ± 0.5 ns, the degradation is quite flat over the frequency. Therefore using this correlation time, the slight oscillator drift which may occur would not cause a serious performance degradation.

Another important characteristic for the sinusoidal template is the timing error. Figure 3.7 shows the comparison of the second derivative Gaussian model and sinusoidal template as a fuction of time mismatch for f_c=1.25 GHz. As shown in this

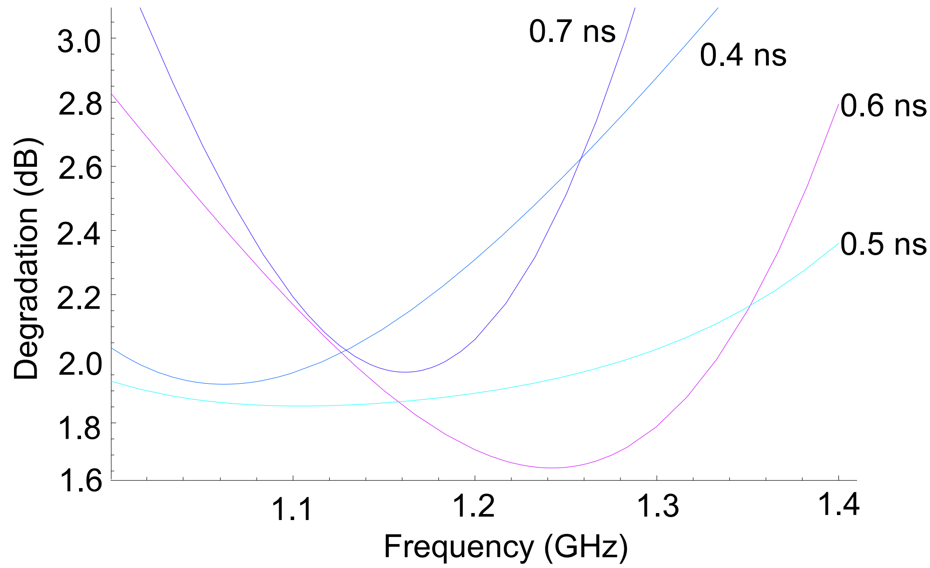

Figure 3.6: The output SNR degradation by the Template frequency

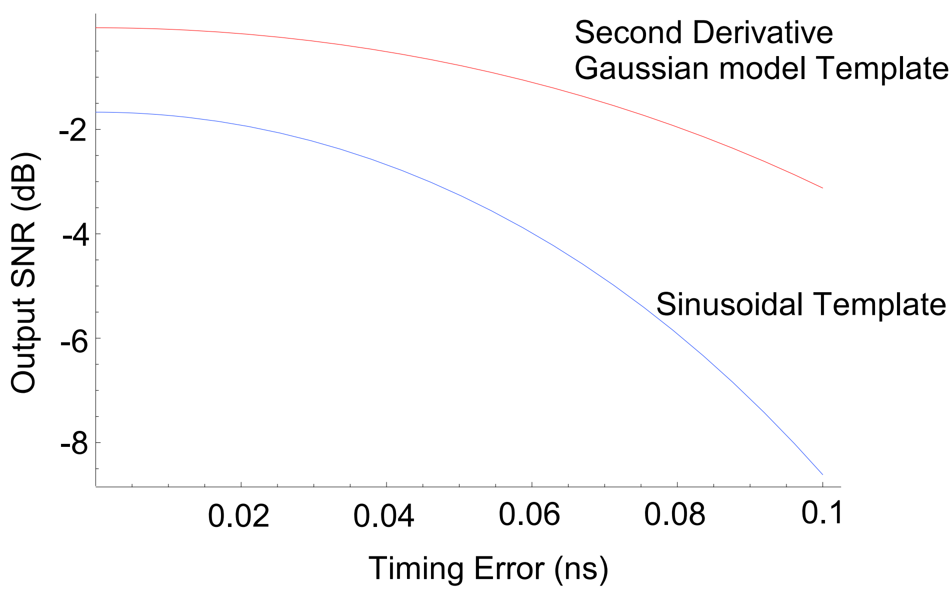

Figure 3.7: Comparison of Output SNR degradation by timing error.

figure, the correlator using the second derivative Gaussian model template is less sensitive to timing error than the correlator using a sinusoidal template.

3.2 UWB System Structure

Using the sinusoidal template, the UWB receiver structure can be simpler than when using the second derivative Gaussian model template. A basic analog phase locked loop (APLL) type UWB system is shown in the figure 3.8 a). With a sinusoidal template and properly derived choices for T_f and T_c in the TH signal format, the UWB system can have the same structure as the APLL [21]. The modifications from the real APLL are the switch between the multiplier and the integrator, and the sample and hold (S/H) block at the end of the system. This switch controls the correlation time with respect to the hopping sequence. When the switch is on, the incoming signal correlates with the sinusoidal template. After the correlation, when the switch is off, the integrator works as the signal holder. The S/H block holds the correlated signal before the correlation output is reset as shown in figure 3.8 b).

The VCO keeps generating template signal with same frequency that occurs when the switch was on. Therefore the correlation output signal locks on the optimal template frequency output of the VCO. Another advantage of this system is that the VCO provides the optimal clock signal to the microprocessor which controls the time hopping sequence and integration time. The bottom half of the autocorrelation loop in figure 3.8 ensures that the output of this system keeps the optimal SNR.

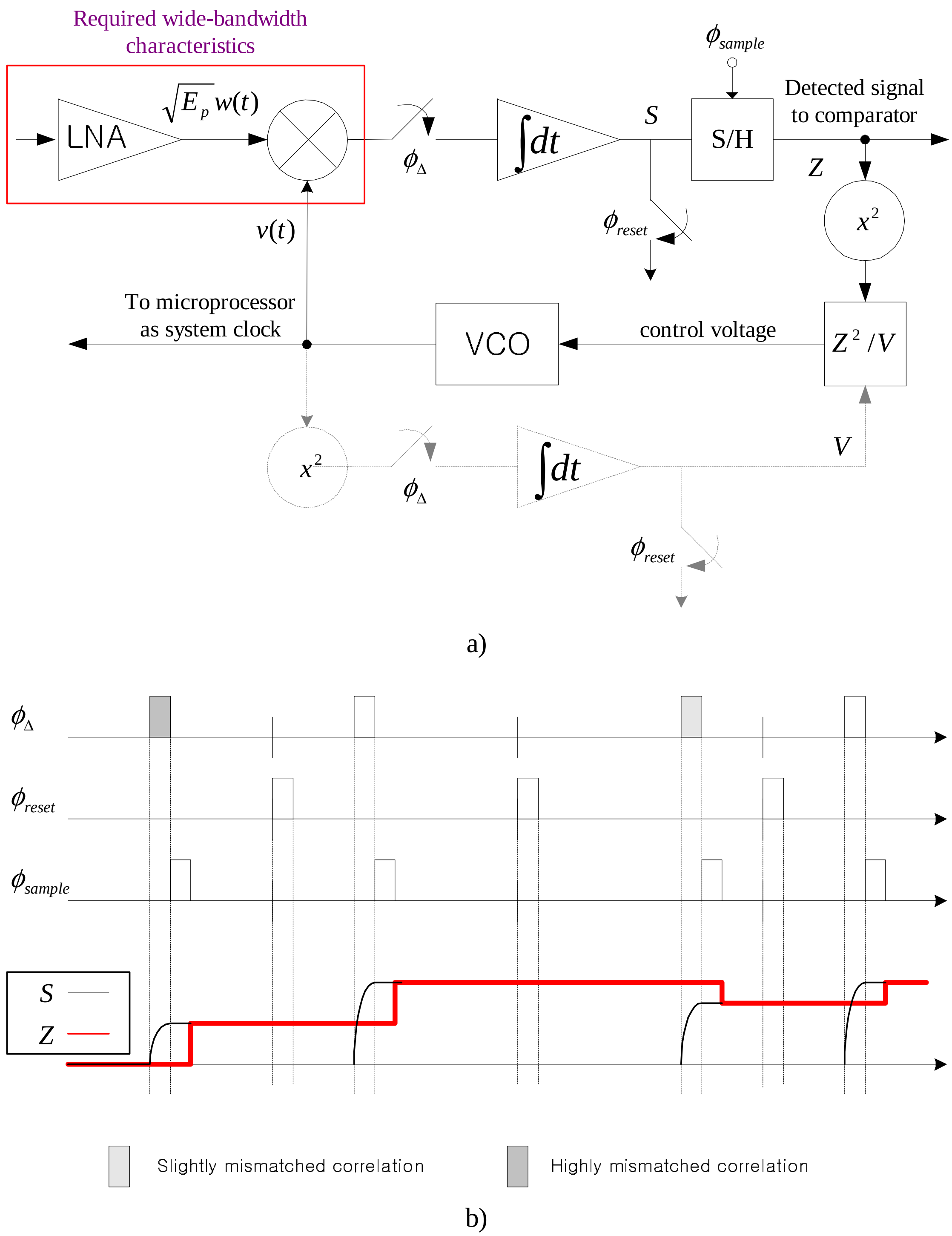

Figure 3.8: a) Simplified UWB receiver using a modified analog PLL b) Timing clock and transient signals at probes.

As described in the equation 3.3, because the SNR is not only related with the correlation function of incoming signal and the template signal but also related with the autocorrelation of the template, the autocorrelation loop for the template is required to achieve the maximum SNR. However because the integration timing clock is operated with respect to the VCO output, the autocorrelation of the template is not considerably changed. Therefore the autocorrelation signal of the sinusoidal template can be replaced with a constant value.

This type of system, it can easily expect that this system does not require much special component. Most of components which are used in this system can be imported from the current technology except for a few key UWB components such as the LNA and mixer that is the part of correlator. The VCO in the system generates a signal with a specific frequency. The integrator follows the UWB system's frame time which is not very fast. However the LNA and mixer are quite different from current narrow bandwidth technology. Since current RF systems employ a narrow bandwidth signal, the narrow bandwidth LNA and mixer can not be applied to the UWB's LNA and mixer. Wide bandwidth LNA can be found on board level designs which are used in Base stations and radar systems, but it's hard to find them on the chip level.

In the remaining chapters, the wide bandwidth LNA and mixer will designed for the UWB system.

Chapter 4

Low Noise Amplifier for Ultra-wide-bandwidth System

The low noise amplifier(LNA) is the first block of a wireless receiver. Its main function in the receiver is to provide enough gain to overcome the noise of subsequent stages. In other words, this LNA gives signal amplification, without any degradation of signal to noise ratio(SNR), and its noise figure determines the lower bound on the system's minimum detectable signal level. Other considerations in LNA design are large signal accommodation without distortion, and impedance matching to the input source over the desired frequency range. In this chapter, starting with a review of recent LNA design, one possible ultra-wide-bandwidth LNA is presented with its analysis.

4.1 LNA Topologies

During last decade, many LNA technologies have been developed. However most of these topologies are constructed for narrow-bandwidth systems because there were no systems that use over a few hundred megahertz of bandwidth. Therefore it is challenging to find a suitable LNA topology for an UWB system.

4.1.1 Survey of Current LNA

For an LNA system, a resistive impedance matching between the LNA and the driving source is a critical requirement. However because the input of the LNA system is connected to a capacitive node, providing good impedance matching to the source without degrading the noise performance is difficult. Therefore various matching methods have been studied to improve LNA performance. Based on these matching methods, the LNA topology can be distinguished as shown in figure 4.1. The first topology, the resistive termination, is a straightforward matching method. The 50Ω resistance directly connected to the input node of a common source amplifier. This connection means that the source can see only the 50Ω resistor over reasonably broadband. However this resistance which is connected directly to the input terminal adds thermal noise of its own and attenuates the signal ahead of the transistor. These effects usually produce an unacceptably high noise figure. Therefore this resistive termination topology is rarely used in LNA design.

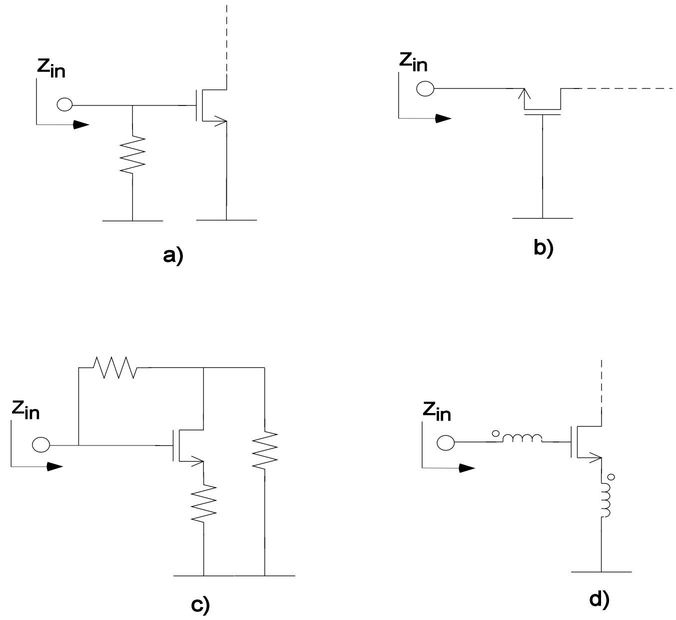

Figure 4.1: LNA topologies. (a) Resistive Termination. (b) $1/g_m$ Termination. (c) Shunt-Series Feedback. (d) Inductive Degeneration.

For the second topology, the $1/g_m$ termination as shown in the figure 4.1 (b), the impedance is set by the $1/g_m$ of the transistor in the common gate stage. This architecture is very simple and can easily achieve the correct impedance matching. In addition to the correct matching, this topology looks like a good choice for a wide-bandwidth system because the transistor's g_m is not much effected by frequency. However to make $1/g_m = 50\Omega$, the g_m value is going to be fixed at 20 mS. This means that the gain of this LNA is fixed without increasing output resistance. Also this fixed transistor size critically affects the noise figure of the single transistor system.

In the common gate configuration, the noise figure and the matching are totally depend on the single transistor in the common gate stage. The equation 4.1 shows the noise figure of the single transistor [33].

$$F = 1 + \frac{\gamma}{\alpha} \tag{4.1}$$

where γ is the coefficient of channel thermal noise and α is

$$\alpha = \frac{g_m}{g_{d0}} \tag{4.2}$$

where g_m is transconductance and g_{d0} is the zero bias drain conductance. For the long channel device, $\gamma = 2/3$ and $\alpha = 1$. In the short channel case, the γ is greater than 2/3. According to these numbers, in the best case the noise figure of this $1/g_m$ architecture tend to be more than 2.2 dB. Therefore this topology gives quite wide-bandwidth impedance matching but it has a large noise figure and difficult to achieve high gain.

The third architecture shown in the 4.1 (c) uses shunt series feedback to set the input and output impedances of the system. With this shunt series architecture, the bias point of the input is fixed with the output voltage. Therefore the biasing point of this system is not set to the optimal bias point. This non-optimal biasing point means that this type of system consumes a lot of power to achieve the desired gain. In addition to this, this shunt series feedback architecture has a stability problem

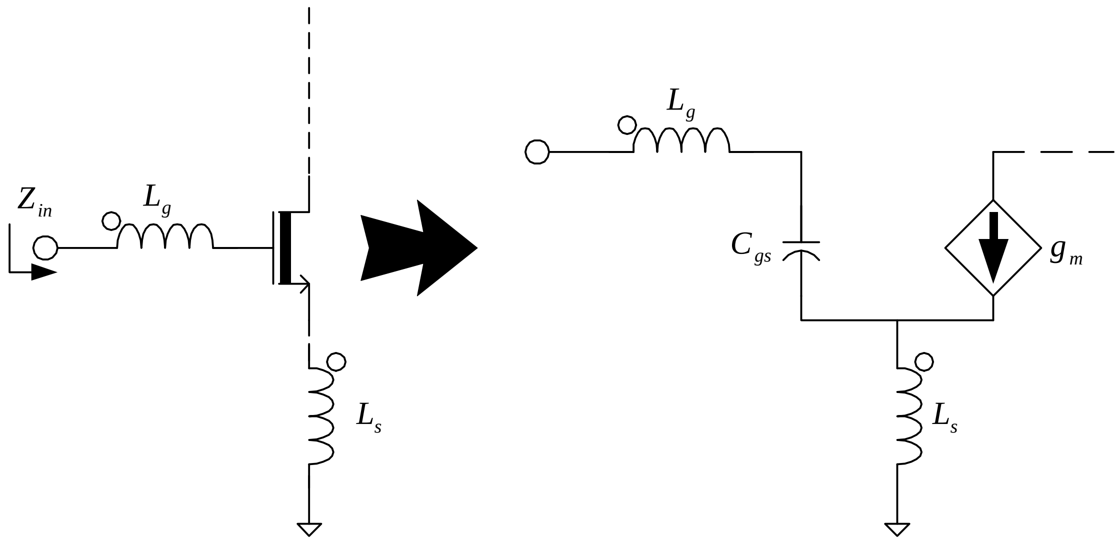

Figure 4.2: The small signal model for the inductive degeneration

because it uses feedback. However this architecture gives good noise figure and wide-bandwidth characteristic for the UWB system.

The last topology in the figure 4.1 (d) is inductive degeneration. This architecture gives very good noise figure and impedance matching for a narrow-bandwidth system. The figure 4.2 is the small signal model for this inductive degeneration architecture. From this small signal model, the input impedance of this architecture can be calculated as

$$\begin{aligned} Z_{in} &= s(L_s + L_g) + \frac{1}{sC_{gs}} + (\frac{g_m}{C_{gs}})L_s \\ &\approx s(L_s + L_g) + \frac{1}{sC_{gs}} + \omega_T L_s \end{aligned} \tag{4.3}$$

At the resonance frequency, the input impedance is purely real and proportional to L_s. Therefore choosing appropriate value of the L_s, the real term can be made

Table 4.1: Recent LNA technology

Author	NF (dB)	Gain (dB)	IP3 (dBm)	Power (mW)	f_0 (GHz)	Architecture	Technology	Year
Huang [9]	1.6	16.4	-7.3	22	0.9	L-Degen	0.25μm CMOS	1999
Janssens [11]	3.3	9	10	10	0.9	L-Degen	0.5μm CMOS	1998
Shahani [34]	3.8	17	-6	12	1.57	L-Degen	0.35μm CMOS	1997
Shaeffer [33]	3.5	22	12.7	30	1.5	L-Degen	0.6μm CMOS	1997
Karanicolas [12]	2.2	15.6	12.4	20	0.9	L-Degen	0.5μm CMOS	1996
Rofougran [30]	3.5	22	na	27	0.9	$1/g_m$ Term	1μm CMOS	1996
Chang [3]	6.0	14	na	7	0.75	R-Term	2μm CMOS	1993
Ko [14]	2	17	na	na	1.57	L-Degen	0.5μm GaAs	1997
Nair [28]	2.5	10	-4	2	0.9	L-Degen	GaAs HFET	1995
Koizumi [18]	5.2	16.7	7.5	28.5	0.95	R-Term	GaAs FET	1995
Benton [1]	2.7	28	na	208	1.6	S.S. FB	GaAs FET	1992
Meyer [27]	2.2	16	6	40	0.9	L-Degen	BiCMOS	1994

equal to the input impedance 50Ω. At this time, the gate inductance L_g is used to set the resonance frequency with L_s which in turn is chosen for input impedance matching purpose. Using this type of architecture, the noise sources are only the transistor's gate resistance and the channel noise. However since this configuration uses resonance at the desired frequency, it can be used only for narrow-bandwidth signals and is not suitable for wide-bandwidth applications.

Table 4.1 shows the results of LNA technologies developed during the 1990's. This table indicates that LNA research, performed mostly on narrow-bandwidth signal, usually used the inductive degeneration method because of its good noise figure and easy input impedance matching. Another interesting phenomenon is that a lot of CMOS LNAs have been studied at the late 1990's. Although the bipolar transistor gives a better noise figure and gain, it also consumes more power and requires more space on the chip than the CMOS transistor. The current trend of most systems is small size and low power solutions. Therefore considering this trend, CMOS architecture is more suitable than bipolar solutions.

Since there are no UWB LNA systems reported in the literature, it is challenging to design the UWB LNA on a chip. Among previous LNAs which have been reviewed, the inductive degeneration method is excluded even though it shows good performance in terms of its good noise figure and impedance matching, because it is designed only for narrow-bandwidth systems. Also the resistive termination method and $1/g_m$ termination should be excluded because of its noise figure and gain limitation. The best choice of the LNA for the UWB system is the shunt-series feedback termination method because it has wide-bandwidth characteristic [27][17][25]. However it still needs some modifications for optimal gain achievement and stability.

4.1.2 LNA for wide-bandwidth Signal

Usually the shunt series feedback can be analyzed with h-parameters because this amplifier is characterized by a current gain. Therefore the input and output relation of this amplifier can be described as

$$\begin{pmatrix} V_1 \\ I_2 \end{pmatrix} = \begin{pmatrix} h_{11} & h_{12} \\ h_{21} & h_{22} \end{pmatrix} \begin{pmatrix} I_1 \\ V_2 \end{pmatrix}. \tag{4.4}$$

From the small signal model shown in the figure 4.3, the H-parameter can be calculated as

$$[H] = \begin{bmatrix} R_f & 1 \\ \frac{g_m R_f}{1+g_m R_s} - 1 & \frac{g_m}{1+g_m R_s} \end{bmatrix}. \tag{4.5}$$

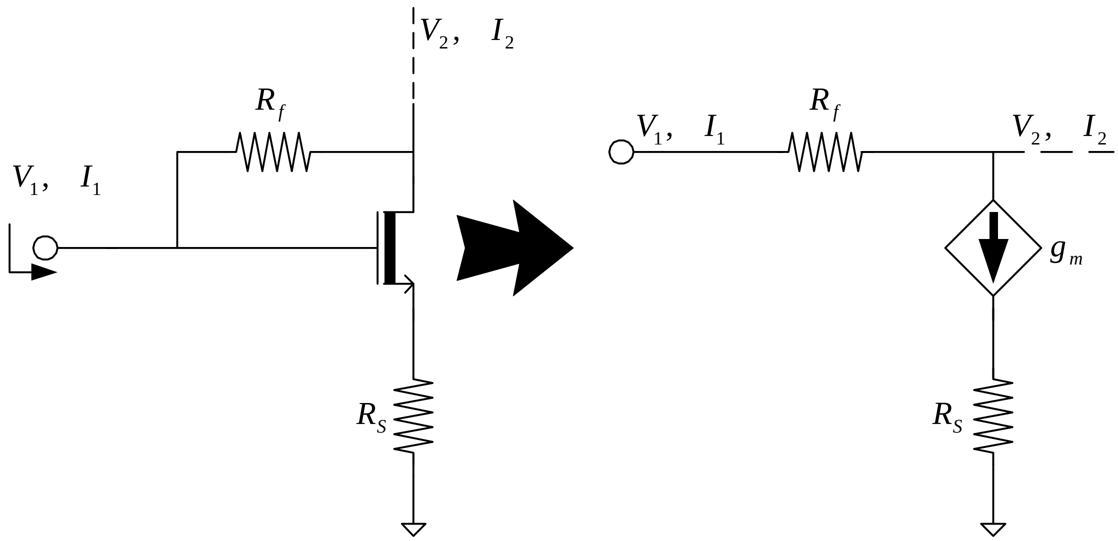

Figure 4.3: Small signal model for the shunt series feedback amplifier

This H-parameter matrix can be converted to the corresponding S-parameter matrix.

$$[S] = \frac{1}{\Delta}\begin{bmatrix} \frac{R_f}{Z_0} - \frac{g_m Z_0}{1+g_m R_s} & 2 \\ 2(1 - \frac{g_m R_f}{1+g_m R_s}) & \frac{R_f}{Z_0} - \frac{g_m Z_0}{1+g_m R_s} \end{bmatrix} \tag{4.6}$$

where $\Delta = 2 + \frac{R_f}{Z_0} + \frac{g_m Z_0}{1+g_m R_s}$. From this S-parameter matrix, considering the ideal matching condition $S_{11} = S_{22} = 0$, the series resistance R_s can be calculated as

$$R_s = \frac{Z_0^2}{R_f} - \frac{1}{g_m} \tag{4.7}$$

Substituting 4.7 onto 4.6 gives S-parameter

$$[S] = \begin{bmatrix} 0 & \frac{Z_0}{R_f+Z_0} \\ 1 - \frac{R_f}{Z_0} & 0 \end{bmatrix} \tag{4.8}$$

As shown in the equation 4.8, the transduced gain S_{21} is flat and perfect matching can be achieved by choosing appropriate values for R_f and R_s. The only limitation of this configuration requires that the source resistance R_s must be nonnegative. If R_s becomes negative this system will oscillate. Therefore this restriction fixed the minimum g_m value of the transistor with desired transduced gain S_{21}. This relationship between g_m and S_{21} can be described as

$$g_m \geq g_{m_{min}} = \frac{R_f}{Z_0^2} = \frac{1 - S_{21}}{Z_0} \tag{4.9}$$

Therefore a transistor satisfying the condition of equation 4.9 can be selected in the negative feedback configuration.

However, this analysis is applicable only for low frequencies where all reactance components can be neglected. In the real circuitry, parasitic components must be taken into account. In the case of UWB systems, the parasitic capacitance and inductance can not be neglected because the signal is spread out over wide RF range. In addition to this, the bias point of this system should be adjusted. With this configuration, it requires very high power consumption to increase the gain because the bias point of the system is fixed at the output voltage, which is not the optimal DC biasing point.

Because of these undesired effects of parasitic, reactance components and non-optimal dc bias point, the gain is degraded at high frequency as shown in the figure 4.4. According to this figure, not only the gain degradation occurs but also the noise

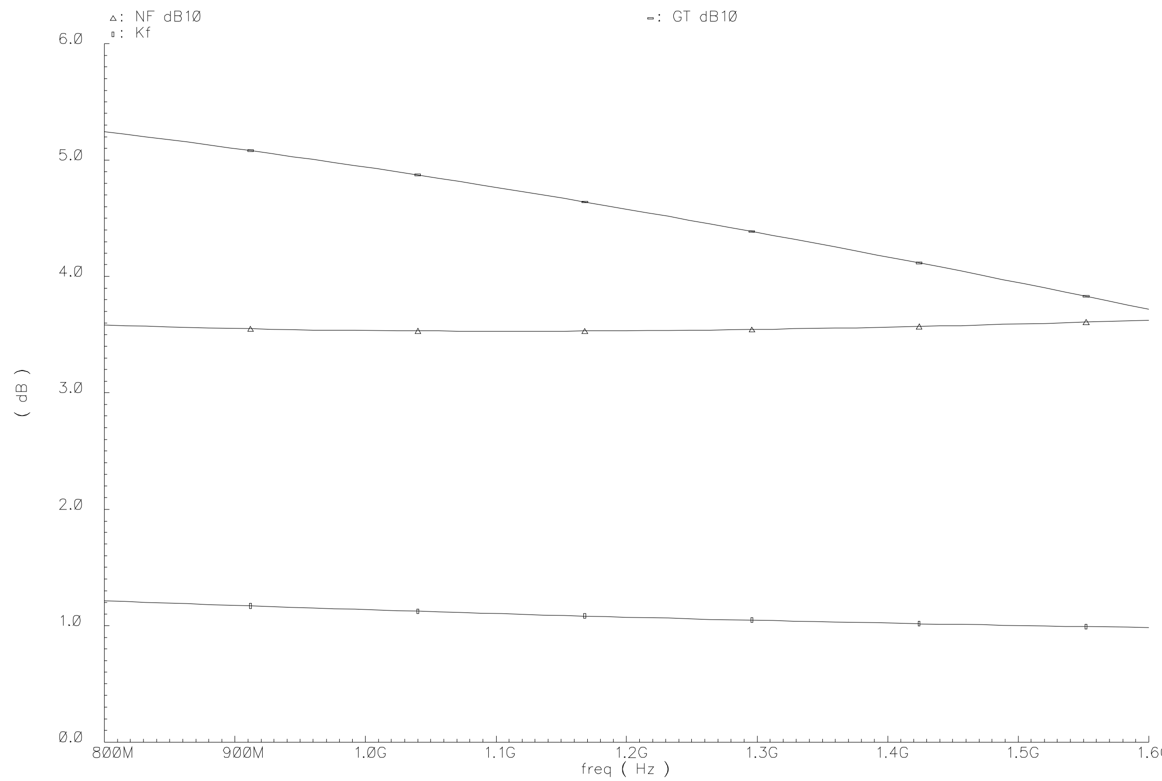

Figure 4.4: LNA transduced gain, noise figure and its stability factor with original shunt series feedback configuration at high frequency.

figure of this configuration is high and the stability drops to the unstable region because of the feedback effect. Therefore this type of configuration requires improve its high frequency gain and noise figure without loosing stability. In the following section, the requirements of the wide-bandwidth LNA are going to be stated along with the wide-bandwidth LNA design and its analysis.

4.2 Design and Analysis of a Wide-Bandwidth LNA

As shown in the previous section, the shunt series feedback topology is a suitable architecture for the UWB system. However this architecture still requires some improvement at high-frequencies. In this section, the modified shunt series feedback LNA will be introduced and analyzed.

4.2.1 Wide-Bandwidth LNA Design

To design a wide-bandwidth LNA, there arise a few considerations in addition to general LNA design criteria. The following items are the general LNA design considerations.

- Gain and gain flatness (in dB)
- Operating frequency and bandwidth (in Hz)
- Output power (in dBm)

- Power supply requirement (in V and A)
- Input and output reflection coefficients (VSWR)
- Noise figure (in dB)

Besides of these considerations, in wide-bandwidth amplifier design, there are a few more problems that must be solved. One of the major problems in the wide-bandwidth amplifier design is the limitation imposed by the gain-bandwidth product of the active device. Any active device has a gain roll off at high frequency because of the gate-drain and gate-source capacitance in the transistor. This effect degrades the forward gain $|S_{21}|$ as the frequency increases and eventually the transistor stops functioning as an amplifier at the transition frequency f_T. In addition to this $|S_{21}|$ degradation as frequency increases, other complications that arise in wide-bandwidth amplifier design include:

- Increase in the reverse gain $|S_{12}|$, which degrades the overall gain even further and increases the possibility for the circuit to fall into oscillation.
- Frequency variation of S_{11} and S_{22}.
- Noise figure degradation at high frequency.

To reduce these effects, the negative feedback configuration, shunt-series feedback configuration, is used in this work. Also, the frequency compensated matching network technique is applied to improve the system's gain flatness.

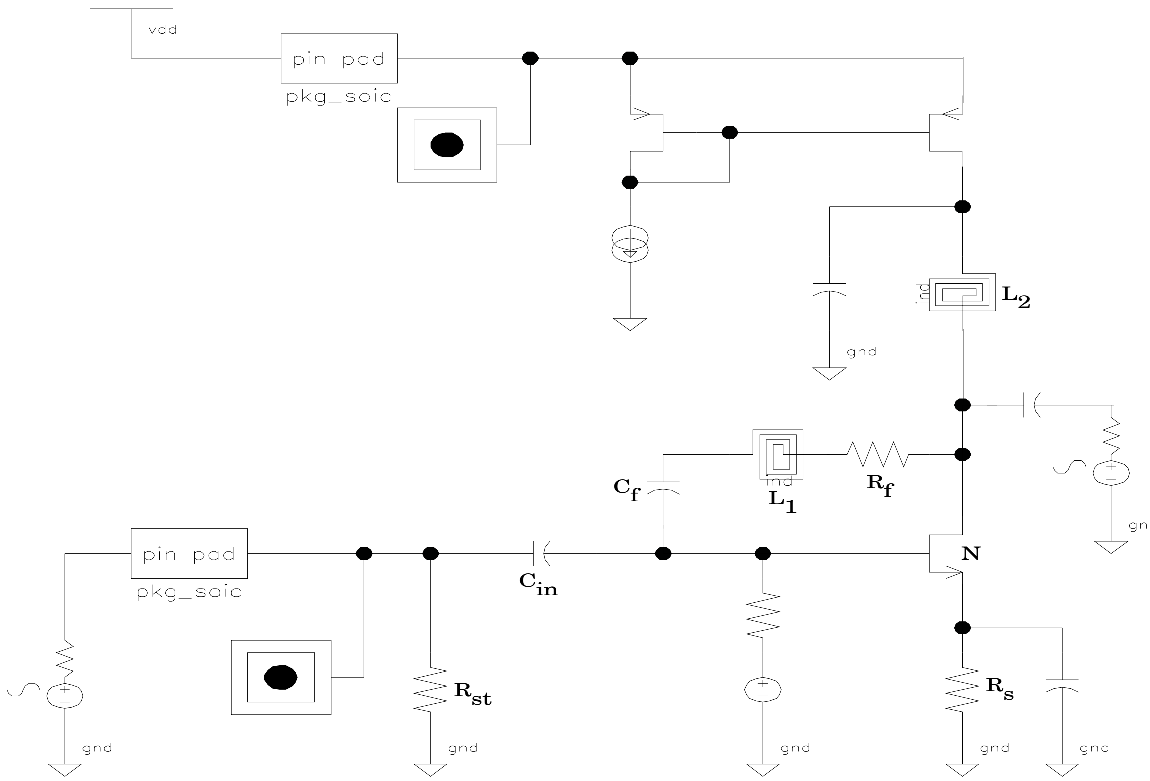

Figure 4.5: The designed ultra wide-bandwidth LNA schematic

The frequency compensated matching network technique uses mismatch on the input or output port of the devices to compensate for the frequency variations. With this technique, the impedance of input or output port is frequency dependent. This means that the input signal can not have maximum power transfer over the desired frequency range. Also to use this technique, the system gain circle at the higher frequency must be inside of the gain circle at the lower frequency in the smith chart. Therefore this technique is used for analyzing flat gain amplifier design.

With these considerations, the UWB LNA has been designed as shown in figure 4.5. In this figure, the load inductance L_2 replaces the resistive load of the original shunt series feedback configuration. The magnitude of the inductor's impedance

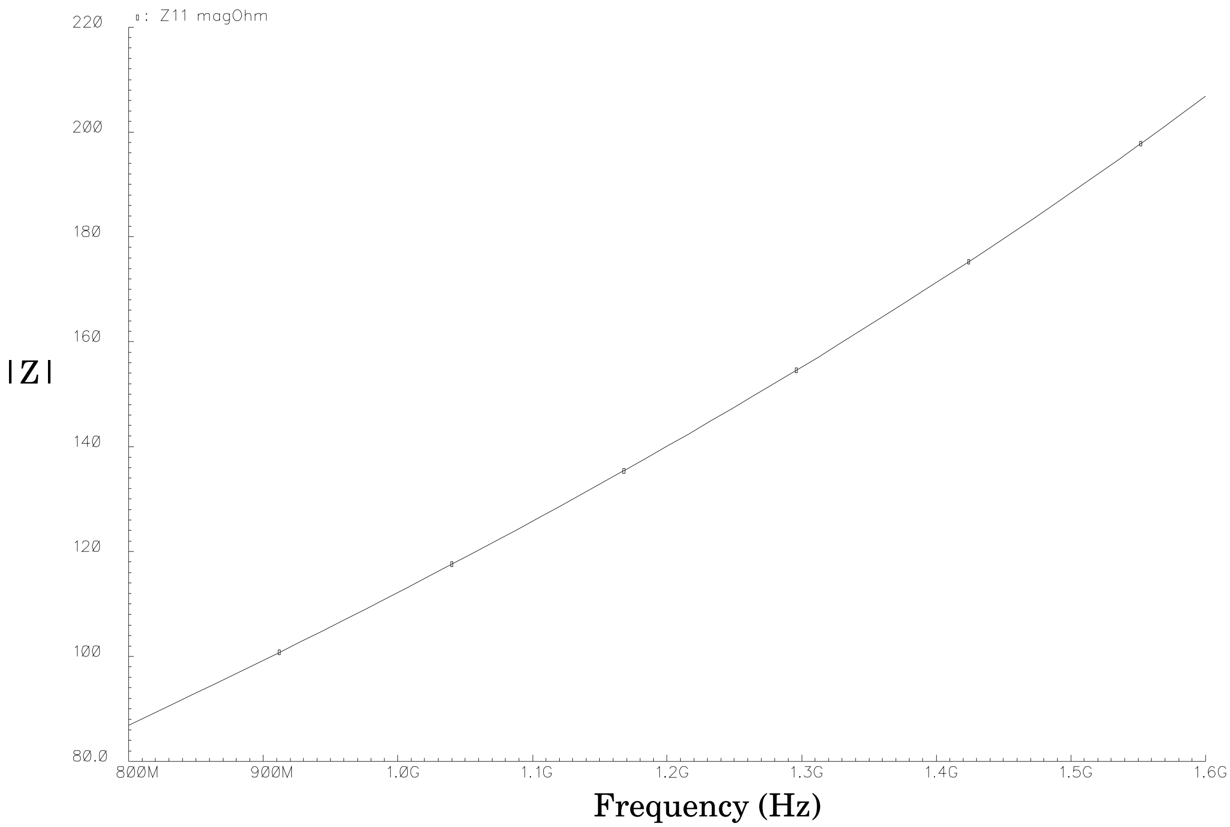

Figure 4.6: Magnitude of inductor impedance vs. frequency (at L = 15.8 nH and Q-factor included)

increases as frequency increases as shown in figure 4.6. This increased inductor's impedance compensates for the amplifier degradation that occurs as frequency increases. With this inductor load, the resonant frequency must be outside of the operating frequency range or this amplifier becomes a narrow-bandwidth amplifier. Although the load inductor increases the higher frequency gain, it still is not enough to achieve gain flatness because it is very difficult to design the on-chip inductor that has large enough inductance to cover the loss in gain at high frequencies. Also with a very large inductor, the inductor's self-resonance frequency is quite low.

To give additional gain at higher frequencies, the inductor L_1 has been added. From the equation 4.8, the magnitude of the forward gain S_{21} is feedback resistance R_f. However this R_f value can not be excessively increased because of the restriction described in the equation 4.7. A large increment of R_f causes R_s to be negative, which it results in system oscillation. However added inductance L_1, does not affect R_s but it adds more impedance, which results in get more gain at high frequency.

Another important component is the DC blocking capacitance C_f. This capacitance blocks the DC current that comes from the output node. This blocking separates the input and output voltage level. Therefore it becomes possible to achieve the optimal biasing point of the transistor N, and maximize the transistor's g_m. This effect reduces the power consumption of the system and increases the gain. The result of this configuration is plotted on figure 4.7. As shown in this figure, the transduced gain of this system has about 8.5 dB and variation of ±0.2 dB over the operational frequency range. The noise figure of this system is about 3 dB and the stability factor indicates this system is unconditionally stable in working frequency range.

4.2.2 Stability Consideration

Stable performance in the frequency range of interest is the first requirement of amplifier design. In case of a feedback amplifier, this stability is the most important

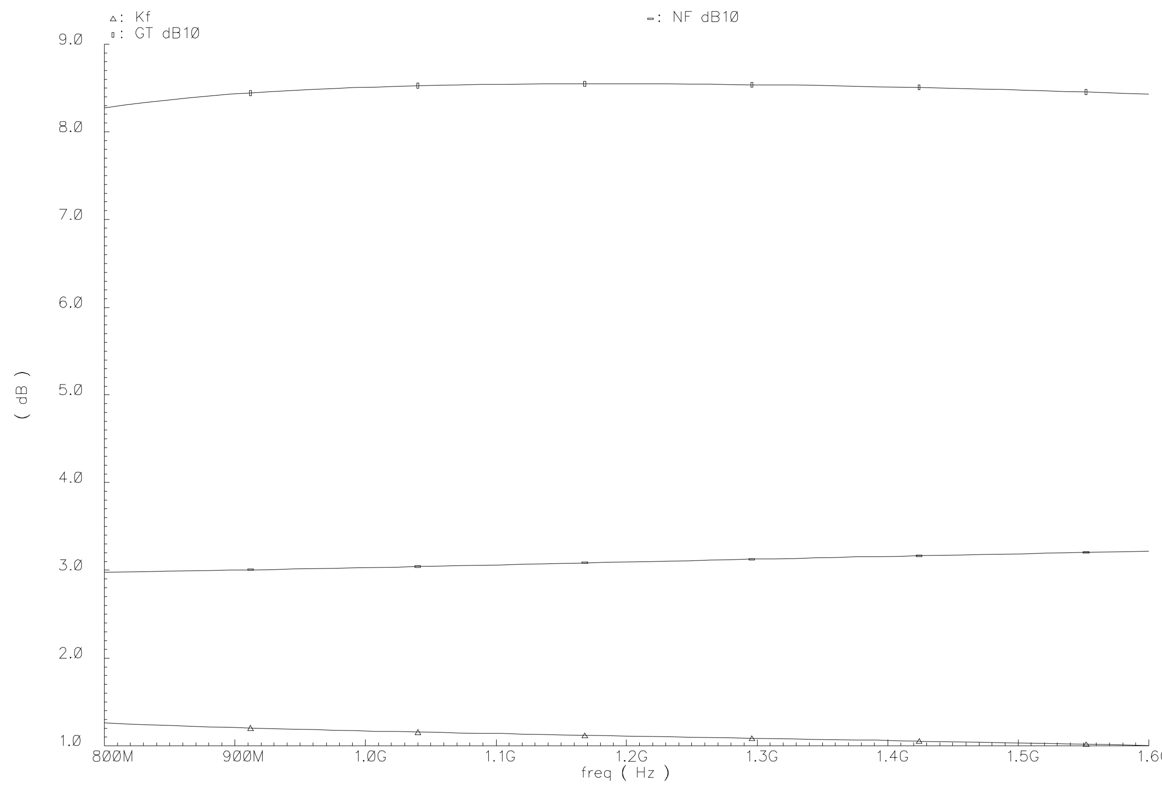

Figure 4.7: The forward gain, Noise figure and the system stability factor for the UWB LNA

factor to be considered. In most of RF circuits, this stability is related to a reflection at a certain frequency. In other words, depending on operating frequency and termination, the stability of a system can be determined.

In a two-port system, the reflection coefficients can be described with S-parameters.

$$|\Gamma_{in}| = \left|\frac{S_{11} - \Gamma_L \Delta}{1 - S_{22}\Gamma_L}\right| < 1 \tag{4.10}$$

$$|\Gamma_{out}| = \left|\frac{S_{22} - \Gamma_S \Delta}{1 - S_{11}\Gamma_S}\right| < 1 \tag{4.11}$$

where the $\Delta = S_{11}S_{22} - S_{12}S_{21}$. $|\Gamma|$ can be represented by a circle in the Γ plane, which is called a stability circle. The input stability circle can be described as

$$(\Gamma_S^R - C_{in}^R)^2 + (\Gamma_S^I - C_{in}^I)^2 = \left(\frac{|S_{12}S_{21}|}{||S_{11}|^2 - |\Delta|^2|}\right)^2 = r_{in}^2 \tag{4.12}$$

where

$$C_{in} = C_{in}^R + jC_{in}^I = \frac{(S_{11} - S_{22}^*\Delta)^*}{|S_{11}|^2 - |\Delta|^2}, \tag{4.13}$$

and the output stability circle can be described as

$$(\Gamma_L^R - C_{out}^R)^2 + (\Gamma_L^I - C_{out}^I)^2 = \left(\frac{|S_{12}S_{21}|}{||S_{22}|^2 - |\Delta|^2|}\right)^2 = r_{out}^2 \tag{4.14}$$

where

$$C_{out} = C_{out}^R + jC_{out}^I = \frac{(S_{22} - S_{11}^*\Delta)^*}{|S_{22}|^2 - |\Delta|^2}. \tag{4.15}$$

To make the system stable, the source and load reflection coefficients must be in stable region. This stable region can be described as intersection of the load reflection coefficients circle and input stability circle and intersection of the source reflection coefficients circle and output stability circle as shown in equations 4.16 and 4.17.

$$\text{Source stable region} = \begin{cases} \{|\Gamma_S| < 1\} \cap \{|\Gamma_{out}| > 1\} & \text{if } |S_{22}| < 1 \\ \{|\Gamma_S| < 1\} \cap \{|\Gamma_{out}| < 1\} & \text{if } |S_{22}| > 1 \end{cases} \tag{4.16}$$

$$\text{Load stable region} = \begin{cases} \{|\Gamma_L| < 1\} \cap \{|\Gamma_{in}| > 1\} & \text{if } |S_{11}| < 1 \\ \{|\Gamma_L| < 1\} \cap \{|\Gamma_{in}| < 1\} & \text{if } |S_{11}| > 1 \end{cases} \tag{4.17}$$

Using these conditions, the stability analysis requires too much attention to avoid unstable region. Therefore it is desirable to make the amplifier remain stable throughout the entire domain of the smith chart at the selected frequency range and bias condition. To achieve this unconditionally stable state, when $|S_{11}| < 1$ and $|S_{22}| < 1$, the stability circle must not overlap with $|\Gamma_S| < 1$ and $|\Gamma_L| < 1$. This condition can be described with the following equation derived from the circle equation shown in the equations 4.12 and 4.14.

$$||C_{in}| - r_{in}| > 1 \tag{4.18}$$

$$||C_{out}| - r_{out}| > 1 \tag{4.19}$$

Substituting r_{in} in 4.12 and C_{in} in 4.13 into 4.18, gives the stability factor k.

$$k = \frac{1 - |S_{11}|^2 - |S_{22}|^2 + |\Delta|^2}{2|S_{12}||S_{21}|} > 1 \tag{4.20}$$

where $\Delta = S_{11}S_{22} - S_{12}S_{21}$.

Applying this stability factor k into the UWB LNA design, the frequency dependent stability factor k_f in figure 4.7 has been plotted. As shown in this figure, the stability factor stays above 1, over frequencies of interest. Therefore this system cannot fall into oscillation.

To keep the stability factor in the unconditionally stable region, the stabilization method must be applied in the system. The most simple and effective way to stabilize an active device is to add a series resistance or a shunt conductance to the port. If a source resistance is added to the source port, this resistance increases the real value of the input impedance, resulting in the input impedance becoming positive. For the load port the effect is identical. However adding a serial resistance to a port may add too much noise into the system noise characteristic because the series resistance, which is adding the noise source, is placed in the signal path. Therefore it is recommended to add shunt conductance to the port. In this case, the conductance should be small enough to avoid signal flow. In other words, a large enough shunt resistance should be added to the port. For the UWB LNA design, the shunt conductance R_{st} in figure 4.5 has been added to ensure its stability. This R_{st} has large enough resistivity to not significantly increase the noise in the system.

Figure 4.8 shows stability circles before adding the shunt conductance for the stabilization and figure 4.9 is the stability circles after adding the shunt conductance. As shown in these figures, the source and load stability circles are moved further away from $|\Gamma|$ is 1 by adding the shunt conductance.

4.2.3 Constant Gain Amplifier

To design a amplifier which has constant gain over the operating frequency range, gain terminology should be described first. In RF amplifier design work, the transduced gain often in used as the gain term, unlike other analog amplifiers. This transduced gain is defined as the output power that is delivered to a load by a source, divided by the maximum power available from the source. Transduced gain includes the effects of input and output impedance matching as well as the contribution that the transistor makes to the overall gain of the amplifier stage. This transduced gain is defined [24] as

$$G_T = \frac{\text{power delivered to the load}}{\text{available power from the source}} \tag{4.21}$$

This definition in 4.21 can be described with the S-parameters of the RF amplifier and the source and the load reflection coefficients Γ_S and Γ_L as

$$G_T = \frac{|S_{21}|^2(1-|\Gamma_S|^2)(1-|\Gamma_L|^2)}{|(1-S_{11}\Gamma_S)(1-S_{22}\Gamma_L)-S_{12}S_{21}\Gamma_L\Gamma_S|^2} \tag{4.22}$$

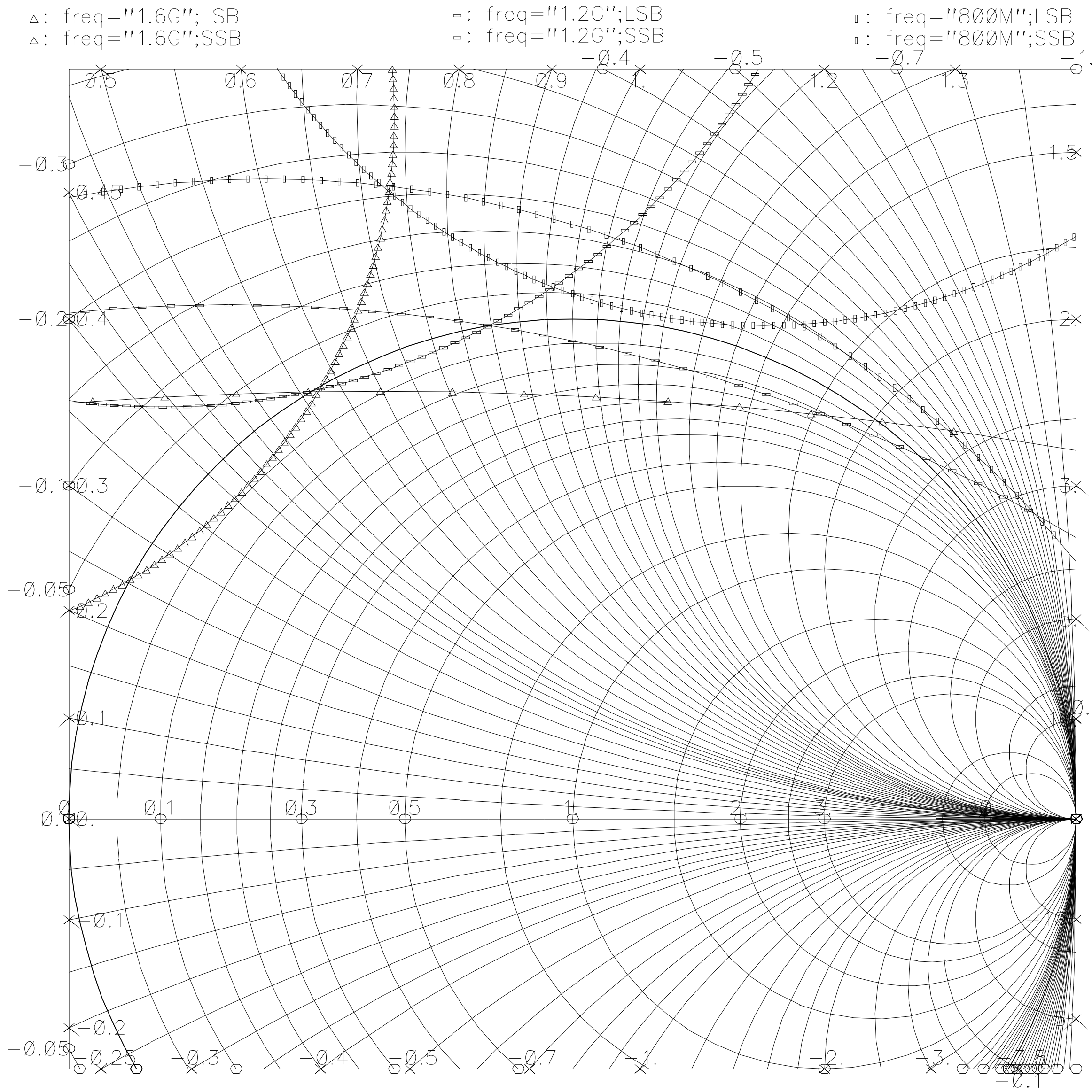

Figure 4.8: The load and the source stability circles on the smith chart before adding the shunt conductance.

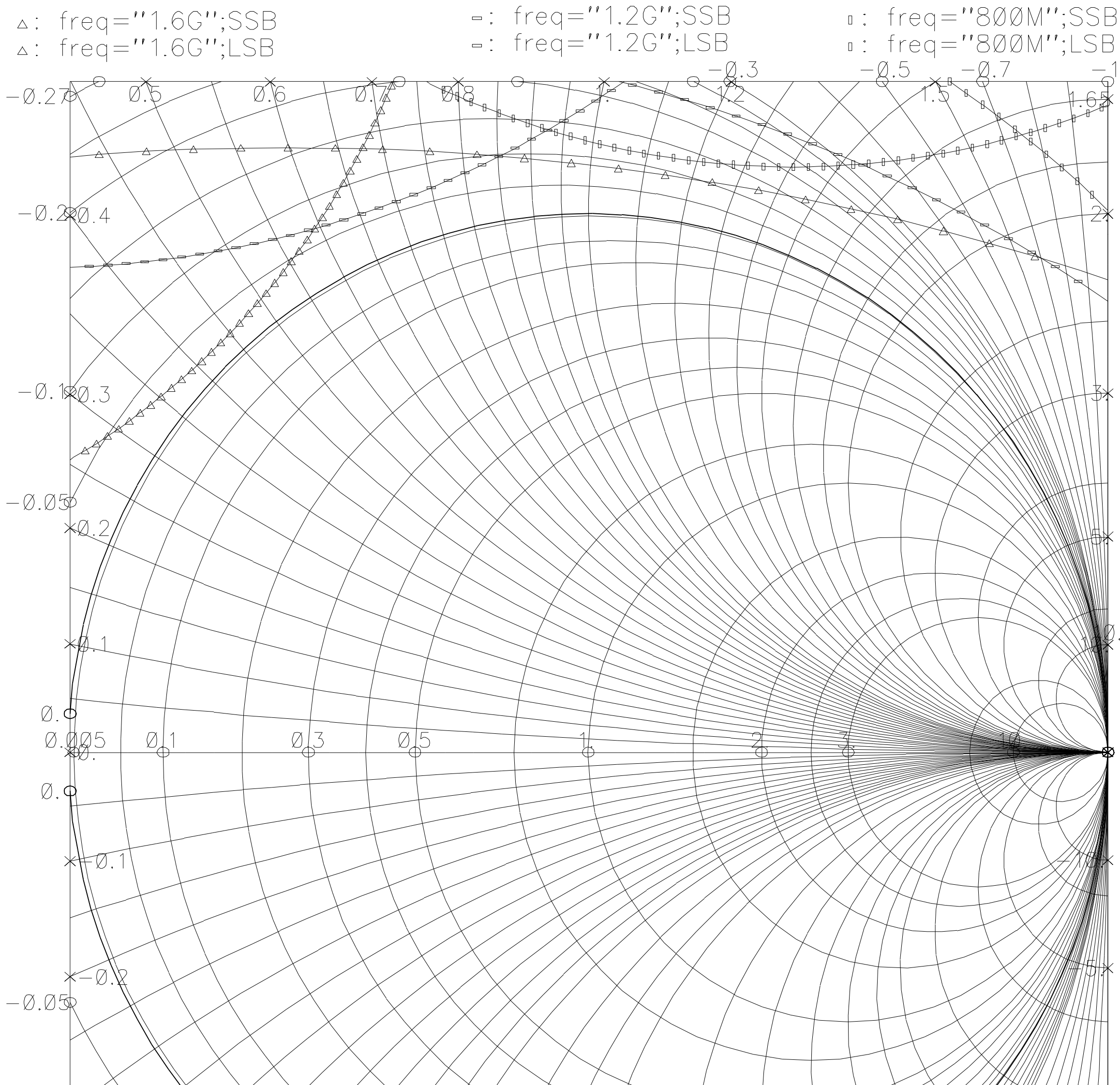

Figure 4.9: The load and the source stability circles on the smith chart after adding the shunt conductance.

When designing a UWB LNA, gain flatness is more important than maximum gain achievement. For a narrow-bandwidth system, usually the LNA is required to achieve maximum gain. This maximum gain can be achieved in the equation 4.22 when Γ_S and Γ_L are 0. However in the UWB system, the transduced gain G_T cannot be the same over the operating frequency range when the reflection coefficients are 0. Therefore it is necessary to fix the transduced gain over the frequency range i.e., it is required to reduce the G_T at some frequencies to achieve flat gain across band. This method has been known as frequency-compensated matching or selective mismatching [15].

Frequency-compensated matching method is simply a manageable way of decreasing gain by not perfectly matching the transistor to its load. This method may not satisfy someone who believes that at RF frequencies, a transistor must be matched to its source and load impedance. However this is not true for a wide-bandwidth system. A transistor is simultaneously conjugate matched to its source and load only if maximum gain is desired, without regard for any other parameters such as bandwidth. In a UWB system, achieving the maximum gain over the operating frequency band is only for the ideal case in which no extrinsic parameters are considered.

The most effective way of selectively mismatching a transistor is through the use of a constant gain circle as plotted on a smith chart. For the UWB system case, plot the constant gain circle of desired gain at various frequencies over the operating band and then move these circles to overlapped positions at the center of the smith chart using external components.

To calculate this constant gain circle, the location of the center and the radius of the circle must be determined. The center r_0 and the radius d_0 can be calculated with the S-parameters of the transistor.

$$r_0 = \frac{GC^*}{1 + DG} \tag{4.23}$$

$$d_0 = \frac{\sqrt{1 - 2K|S_{12}S_{21}|G + |S_{12}S_{21}|^2 G^2}}{1 + DG} \tag{4.24}$$

where

$$G = \frac{|\text{Gain desired}|}{|S_{21}|^2} \tag{4.25}$$

$$C = S_{22} - \Delta S_{11}^* \tag{4.26}$$

$$D = |S_{22}|^2 - |\Delta|^2 \tag{4.27}$$

$$\Delta = S_{11}S_{22} - S_{12}S_{21} \tag{4.28}$$

and K is the stability factor.

Using this constant gain circle, the gain of the UWB LNA has been adjusted to flat over the operational frequency range. Figure 4.10 shows the constant gain circle at 8.5 dB. These gain circles indicate that this system has flat gain at 8.5 dB over the desired frequency range 0.8 GHz through 1.6 GHz. By adjusting the feedback

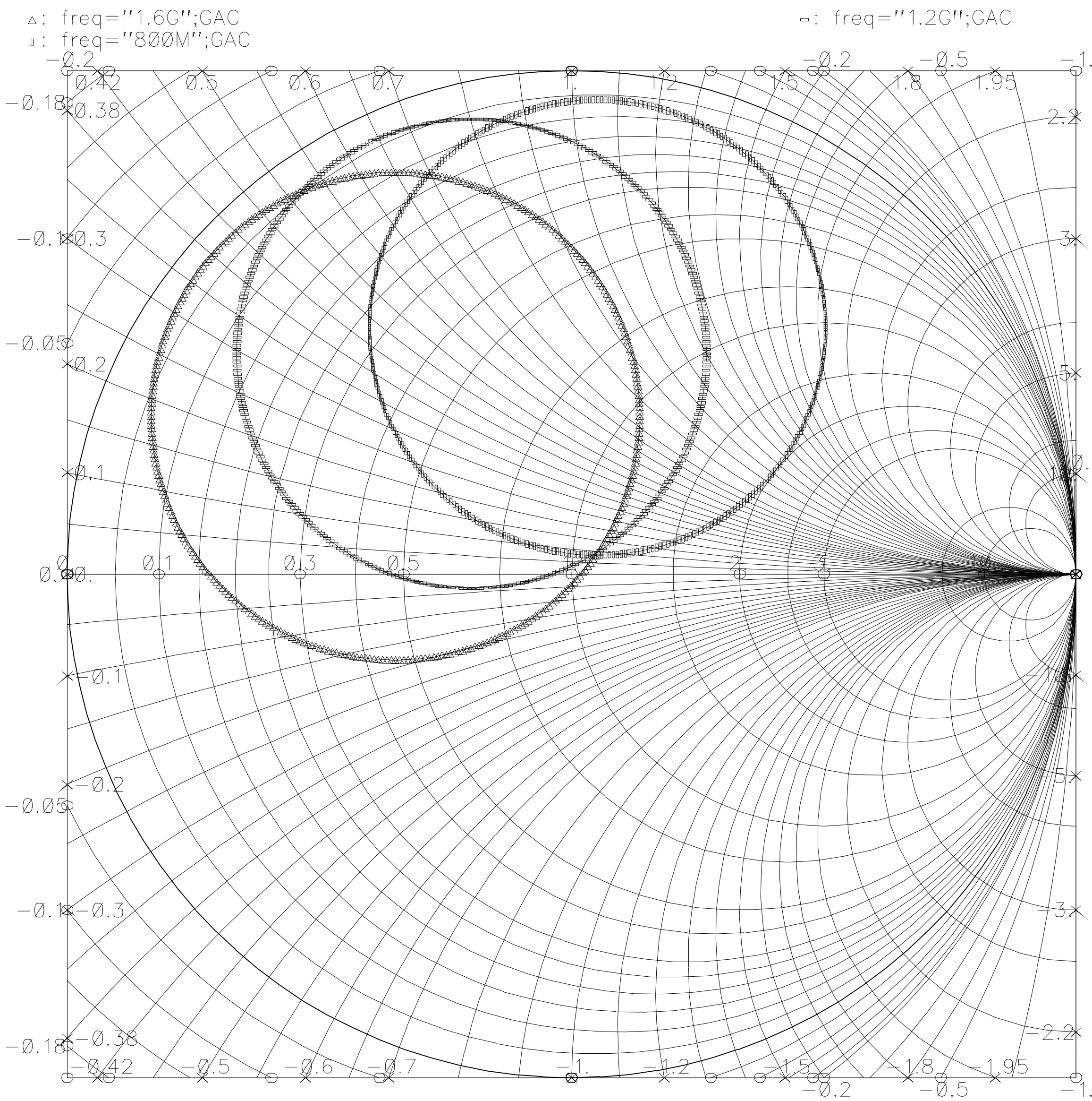

Figure 4.10: Flattened constant gain circles at 8.5 dB over three different frequencies 0.8 GHz, 1.2 GHz and 1.6 GHz

component values of the LNA such as C_f, L_1, and R_f, these circles can be moved to overlap at the center of the smith chart.

4.2.4 Noise Considerations in an LNA

The noise figure of a LNA is an important characteristic of an RF amplifier's performance. For the designed UWB LNA, a major noise source is the source noise which is caused by the source resistance at the input port. Since the UWB LNA uses the frequency-compensated matching method, there are impedance mismatch losses caused by reflected signal. The reflected signal generate noise. Therefore this noise cannot be eliminated for a wide-bandwidth system. The other large noise source is the transistor and the resistance in the feedback loop.

The major noise types in the transistor are flicker noise and thermal noise. Since the frequency range of the UWB system is quite high, flicker noise does not significantly affect system performance. Therefore most of the noise in the transistor comes from thermal noise. This thermal noise has two components:(1) the drain current noise which is generated in the channel, and (2) the gate noise, as shown in figure 4.11.

Recall that the transistor is essentially a voltage controlled resistor. The drain current noise can be described as a resistor noise, as mentioned, in the chapter 2. This drain current noise has been proved for long channel devices operating in the

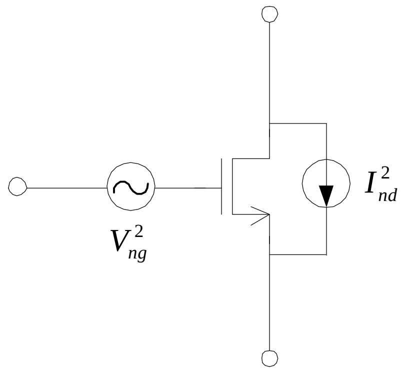

Figure 4.11: Noise sources in a single transistor

saturation region [41]. In the spectral density form, the drain current noise I_{nd}^2 is [37]

$$\overline{I_{nd}^2} = 4kT\gamma g_{ds}B \tag{4.29}$$

where the coefficient γ is equal to2/3 for a long channel transistor. For short channel transistors, this value of γ becomes considerably larger. The g_{ds} in the equation 4.29 is the drain source conductance with $V_{ds} = 0$.

The resistive section of the transistor also generates thermal noise. When a large transistor is used as a LNA, the length of the gate of the transistor becomes very long. This long line of gate poly has resistance and generates thermal noise. To reduce this effects, a fingering method is used in layout [13]. As shown in figure 4.12, this layout technique reduces the gate resistance by a factor of 4 because each gate resistance at the finger is connected in parallel. Therefore with proper layout technique, the thermal noise at the gate, which caused by the gate resistance, can be neglected.

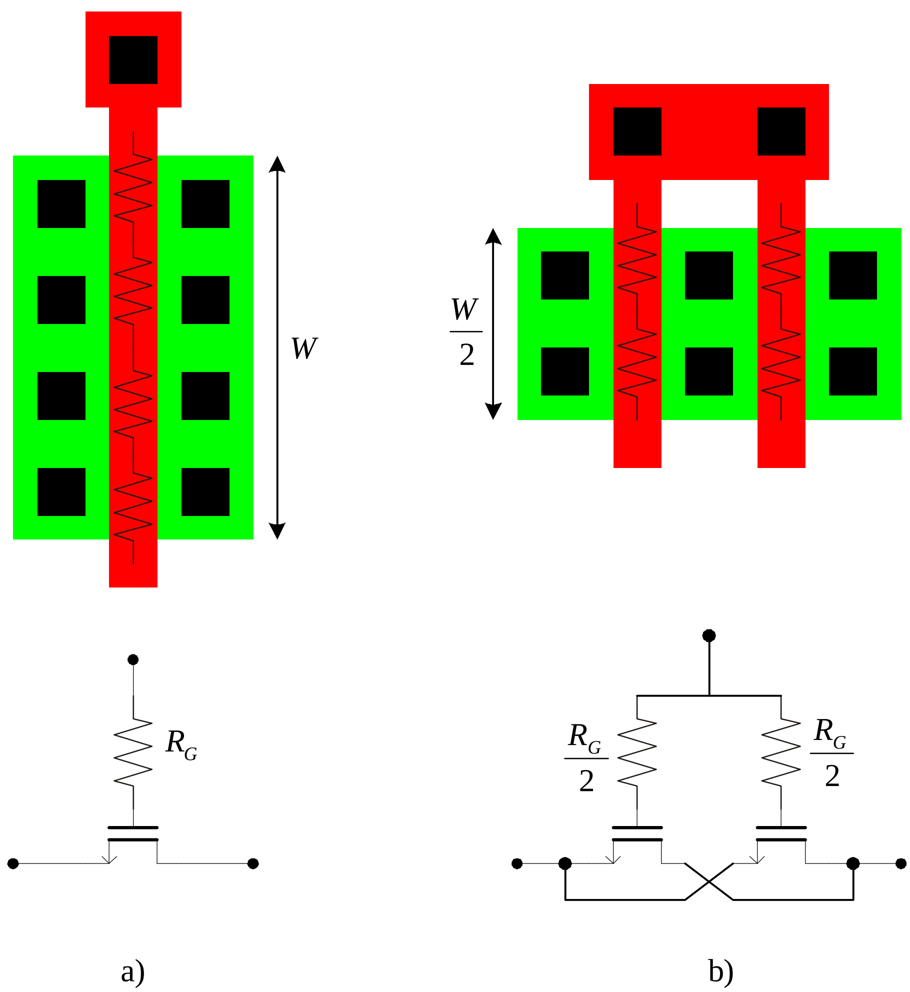

Figure 4.12: Gate resistance reduction by gate fingering

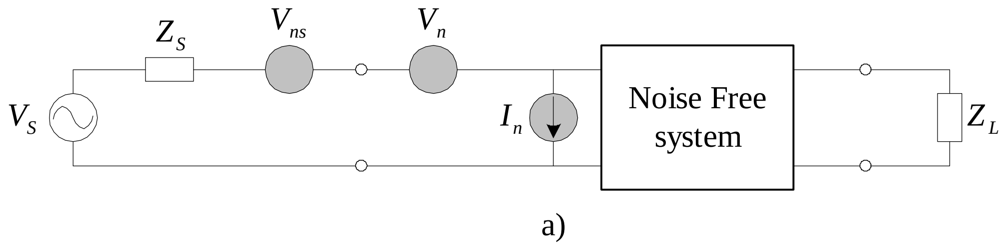

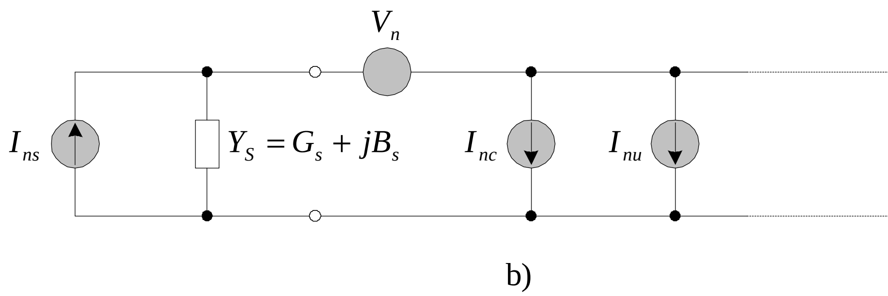

Figure 4.13: a) Generic noise model for noise figure computation b) Noise source model at network input

Considering a noisy LNA system, the main adjustable noise contributors, the transistor noise and the resistance noise in the feedback loop, can be described as a portion of a noisy two-port system. This two-port analysis is a useful noise figure calculation method [46], not only for the shunt series feedback configuration, but also for other systems which can be described as two-port systems. The noise factor in the two-port analysis can be described as [22][42][8]

$$\begin{aligned} F &= F_{min} + \frac{R_n}{G_S}[(G_S - G_{Sopt})^2 + (B_S - B_{Sopt})^2] \\ &= F_{min} + \frac{R_n}{G_S}|Y_S - Y_{Sopt}|^2 \end{aligned} \tag{4.30}$$

The noise parameters in the equation 4.30 are developed figure 4.13. In general, the total noise in the system can be considered as the sum of several source sources of noise. Accommodating the possibility of correlation between V_n and I_n, the total noise power can be separated into two different forms, correlated and uncorrelated. This can be incorporated into the noise model by splitting I_n into an uncorrelated current I_{nu}, and a correlated current I_{nc}. Since the correlated current contribution is related to the noise voltage V_n, defining the complex correlation admittance as $Y_c = G_c + jB_c$,

$$I_{nc} = Y_c V_n \tag{4.31}$$

From the noise factor which is derived from noise power notation

$$F = \frac{\overline{I_{ns}^2} + \overline{V_n^2}(Y_c + Y_s)^2 + \overline{I_{nu}^2}}{I_{ns}^2} \tag{4.32}$$

In equation 4.32, three independent noise sources are represented by an equivalent thermal noise source.

$$\overline{I_{ns}^2} = 4kTBG_s \quad : \quad \text{noise due to the source } Y_s = G_s + jB_s \tag{4.33}$$

$$\overline{I_{nu}^2} = 4kTBG_u \quad : \quad \text{noise due to the equivalent noise conductance } G_u \tag{4.34}$$

$$\overline{V_n^2} = 4kTBR_n \quad : \quad \text{noise due to the equivalent noise resistance } R_n \tag{4.35}$$

Applying these three different noise sources to the equation 4.32, the noise factor becomes

$$F = 1 + \frac{G_u + R_n|Y_s + Y_c|^2}{G_s} = 1 + \frac{G_u + [(G_c + G_s)^2 + (B_c + B_s)^2]R_n}{G_s} \qquad (4.36)$$

To minimize the noise factor, choosing $B_s = -B_c$, the susceptance term $(B_c + B_s)^2$ is zero. Next taking the first derivative of the noise factor with respect to the source admittance G_s, and setting it equal to zero, gives

$$\frac{d}{dG_s}(F|_{B_s=-B_c}) = \frac{1}{G_s^2}\{R_n[2G_s(G_s + G_c) - (G_s + G_c)^2] - G_u\} = 0 \qquad (4.37)$$

which yields the optimal source conductance

$$G_{s_{opt}} = \sqrt{\frac{G_u}{R_n} + G_c^2} \qquad (4.38)$$

Therefore the source admittance $Y_{s_{opt}}$ can be described in terms of the optimal source conductance $G_{s_{opt}}$ and the the correlated susceptance B_c,

$$Y_{s_{opt}} = \sqrt{\frac{G_u}{R_n} + G_c^2} - jB_c \qquad (4.39)$$

With these optimal values, the noise factor can be described minimized form from the equation 4.36.

$$F_{min} = 1 + \frac{G_u}{G_{s_{opt}}} + \frac{R_n}{G_{s_{opt}}}(G_{s_{opt}} + G_c)^2 \tag{4.40}$$

Substituting this equation 4.40 and the $G_u = R_n G_{s_{opt}}^2 - R_n G_c^2$ from the equation 4.38 yields the noise equation 4.30.

In the UWB LNA which has the shunt series feedback structure, there are three different noise sources can be stated, the drain current noise, the gate resistance noise, and feedback resistance noise. Among these noise sources, the gate resistance noise can be disregard by the layout technique as described before. The feedback resistance noise is the unique noise source in feedback system. This noise source increases the system's noise resistance R_n. This increased noise resistance deteriorates the system's noise performance.

4.2.5 Dynamic Range of the UWB LNA

In addition to other LNA characteristics, such as impedance matching, transduced gain, and noise figure, linearity is one of the important factors in LNA design. The role of the LNA in the communication system is not only amplifying the weak RF signal without adding much noise but also maintaining linear operation when receiving weak signal in the presence of a strong interference. The result of loosing linearity causes system desensitization and degrades receiver performance. For current narrow-bandwidth LNA systems, IIP_3 is usually used as a measure of the system's linearity because IIP_3 indicates the interferences between the fundamental frequency and its harmonic frequency. However in a UWB system which uses a very large bandwidth, there is no specified fundamental frequency. Therefore carrier interference with its harmonic frequency does not have meaning. For a the UWB LNA, the gain saturation of the very large input power signal over broad frequency range is more critical. Suppose there is an input signal with very large power and the gain of the LNA system is saturated only in a certain frequency range. Then the system will lose its gain flatness in the working frequency range. This effect causes the system error. Therefore in the UWB system, the lowest 1 dB compression point over the interesting frequency range is the highest limit of the LNA's dynamic range. In most case, the 1dB compression point at the highest frequency of the interesting range is the lowest point.

For the designed UWB LNA, the 1 dB compression point of this LNA at three different frequencies (the lowest, center and the highest of interest) are plotted in figures 4.14, 4.15 and 4.16 respectively. According to simulation results as shown in figures 4.14, 4.15 and 4.16, the input referred 1 dB compression point is about -6 dBm at each figures. Therefore the dynamic range of this LNA system is from the MDS level to -6 dBm of the input power.

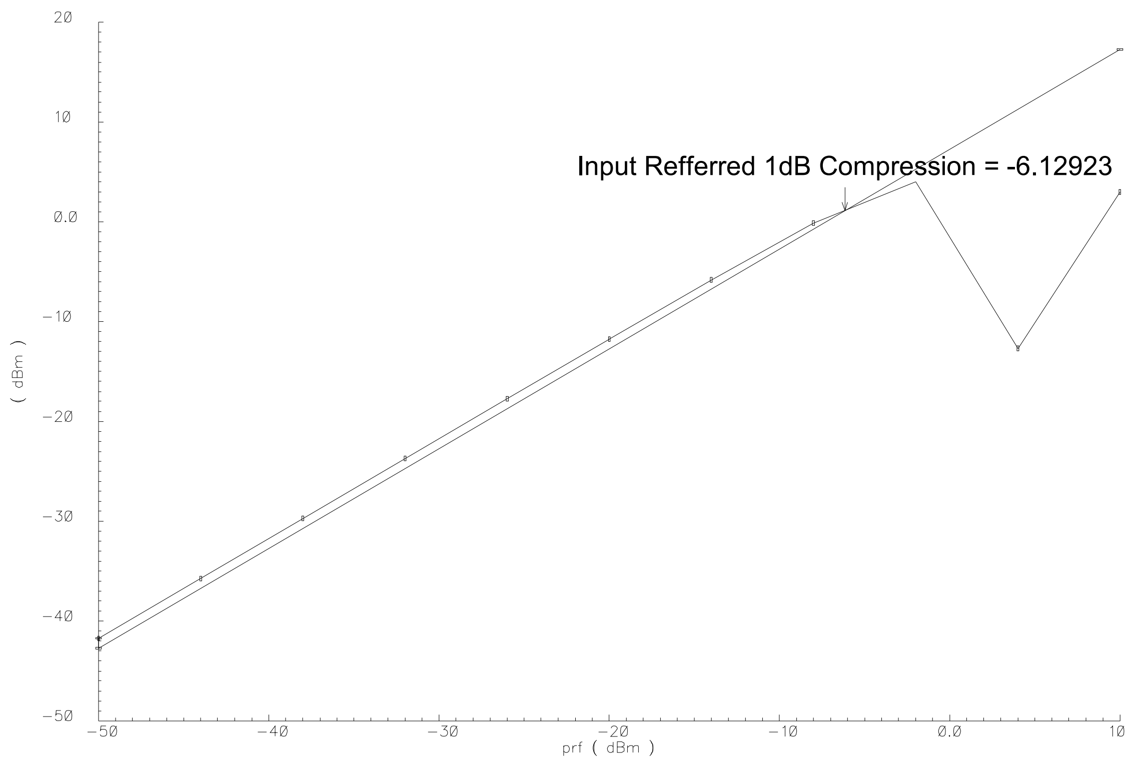

Figure 4.14: 1 dB compression point of the LNA at 0.8 GHz

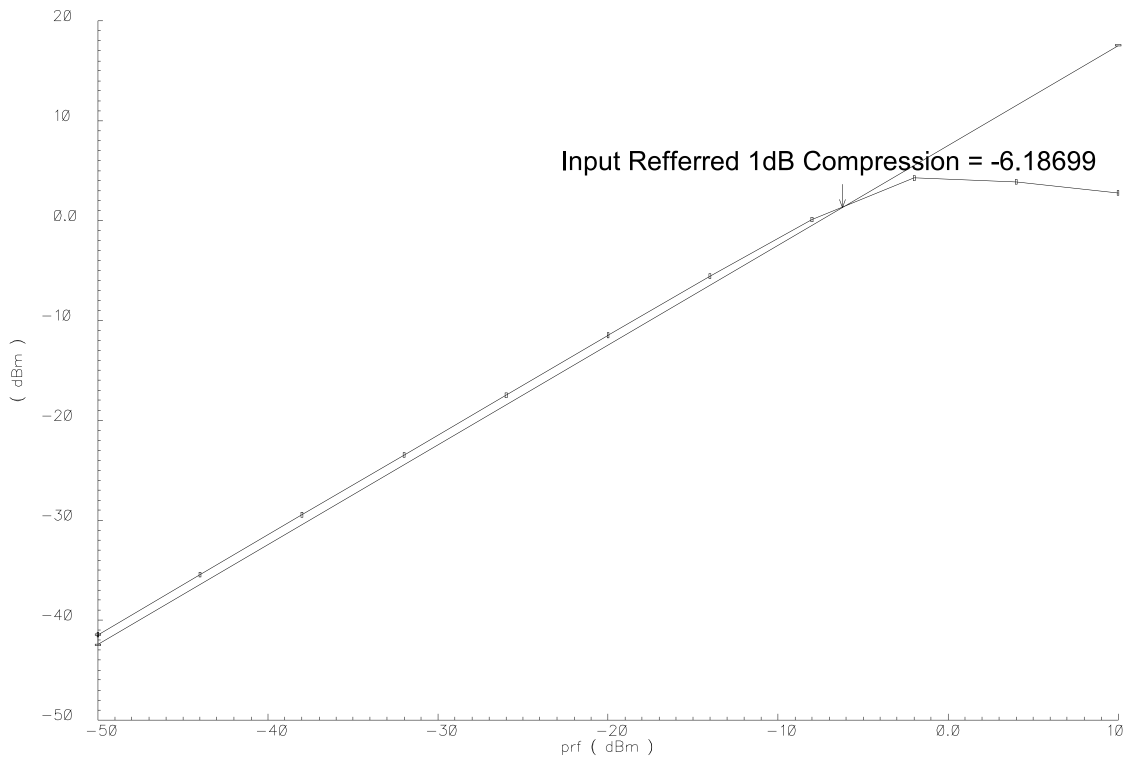

Figure 4.15: 1 dB compression point of the LNA at 1.2 GHz

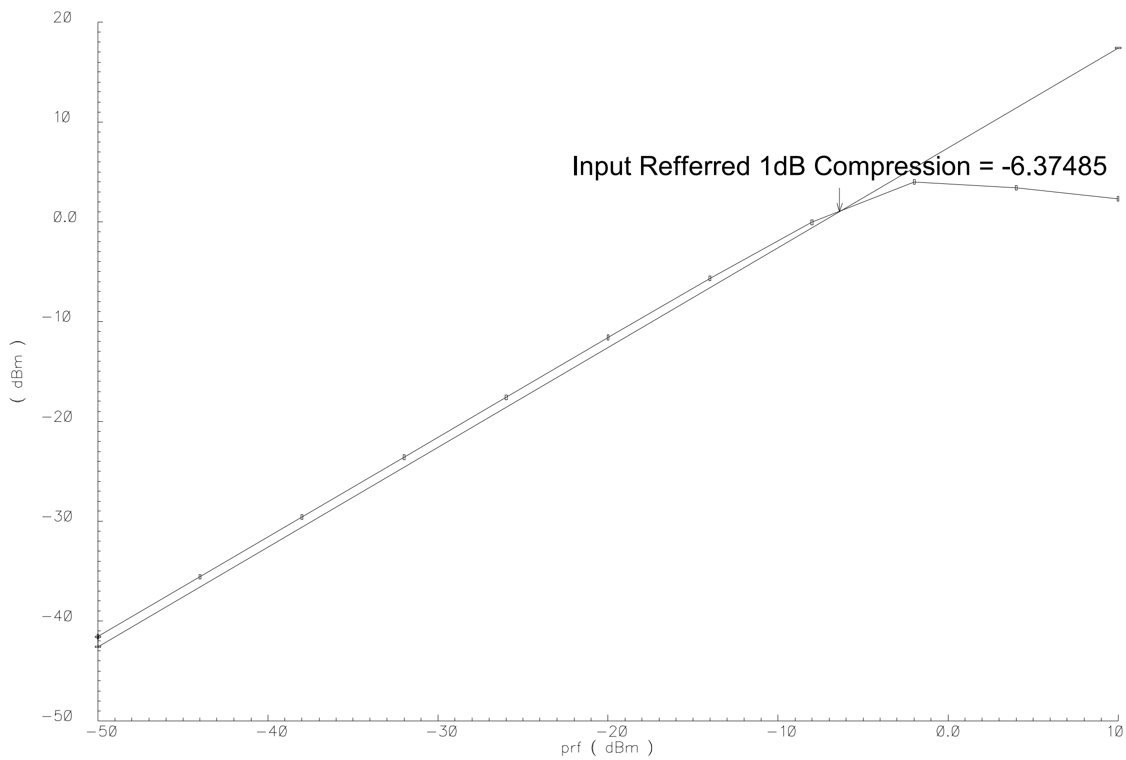

Figure 4.16: 1 dB compression point of the LNA at 1.6 GHz

Table 4.2: The designed LNA performance summary

Operating BW	gain	NF	K	P_{1dB}	Power consumption
0.8 $\sim$ 1.6 GHz	8.4$\pm$ 0.1 dB	about 3 dB	> 1	-6 dBm	23.1 mW

4.3 Summary of the UWB LNA Design

The low noise amplifier for an ultra-wide-bandwidth system has been designed and analyzed. The table 4.2 shows the system performance of this LNA. Although this LNA uses the shunt series feedback configuration, the total power consumption of the system is not high compared to narrow-bandwidth LNAs using the same configuration because this LNA employs an optimal biasing point. Also the load and feedback inductance help to reduce overall system noise figure. However it still has relatively low gain over the frequency range. This low gain problem can be solved two different ways. One is using the cascade LNA and another is using the Mixer's conversion gain. The first approach is quite simple but considering the LNA's power consumption and overall gain, it may require too much resources. Therefore for the UWB system, the mixer's performance is very important.

Chapter 5

Mixer for Ultra-wide-bandwidth System

The mixer is an essential element in all modern radio receivers. In a UWB system, this mixer has a most important role namely to correlate the amplified incoming signal with the template signal. In this chapter, various types of mixers which are currently used in communication systems will be reviewed and a new type of mixer for the UWB system will be introduced.

5.1 Mixer Topologies

In last decade, a variety of mixers have been proposed for communication systems. The basic topologies of these mixers will be illustrated in this chapter for the following four different mixer architectures: subsampling, potentiometric, Gilbert type, and voltage mode.

Table 5.1: The comparison of CMOS Mixers

	Subsampling [35]	Potentiometric [6]	Gilbert type [12]	Voltage Mixer [34]
Power	41 mW	1.3 mW	7 mW	0.5 mW
Conversion Gain	36 dB	18 dB	8.8 dB	-7.3 dB
Noise Figure	47 dB	32 dB	9.2 dB	6 dB
IIP3	-16 dBm	45.2 dBm	-4.1 dBm	4 dBm
Technology	0.6 μm BiCMOS	1.2 μm CMOS	0.5 μm CMOS	0.5 μm CMOS

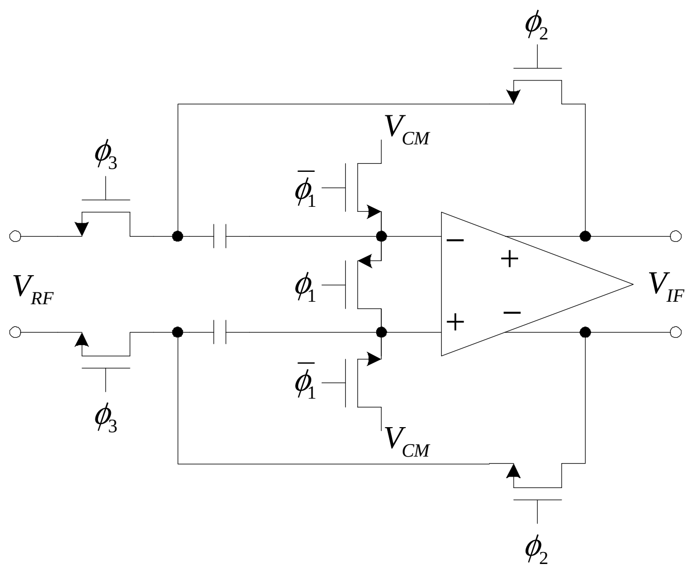

Figure 5.1: Subsampling mixer circuit implementation

5.1.1 Review of Current Mixer Architecture

Table 5.1 briefly describes parameters of the four basic types of mixers, which are currently used for the communication systems. The subsampling mixer performs frequency conversion by sampling the RF signal at a rate greater than the Nyquist rate. The core circuit implementation of this subsampling architecture is illustrated in figure 5.1. As described in table 5.1, the subsampling mixer has an advantage in gain because it can use a high gain operational amplifier at the sampling frequency. However it consumes a large amount of power and has a large noise figure.

Although the subsampling clock frequency is very low compared with the RF signal, clock jitter must be considered, which causes a reduction in the system's SNR [36]. Therefore to reduce this jitter problem, more power must be consumed to generate a precise sampling clock. In addition to this high power consumption problem, this architecture also suffers from a large noise figure because while tracking the incoming signal, this system also tracks and aliases broadband transistor noise.

Since in the UWB system, the signal comes as a sequence of very short pulses in a low duty cycle TH format, the subsampling architecture is not applicable. To sample the UWB pulse which has about a 1 nsec pulse width, the required sampling frequency is at least more than 3 GHz. Generating this high frequency without incurring jitter problems is quite difficult. Therefore this architecture is not suitable for the UWB system's mixer.

The second architecture in table 5.1, the potentiometric mixer in figure 5.2, shows improvement in power consumption, but the noise figure is still quite large. The high noise figure is a consequence of the result of the resistive thermal noise of the input transistors. Basically these transistors at the switching quad are voltage controlled resistances. When the input RF signal is very small, the resistivity of these transistors is large. Hence, the system suffers from a high noise figure. To reduce this noise figure which is caused by the resistivity of input transistors, the high gain LNA must precede this type of mixer, and there is an increase in system power

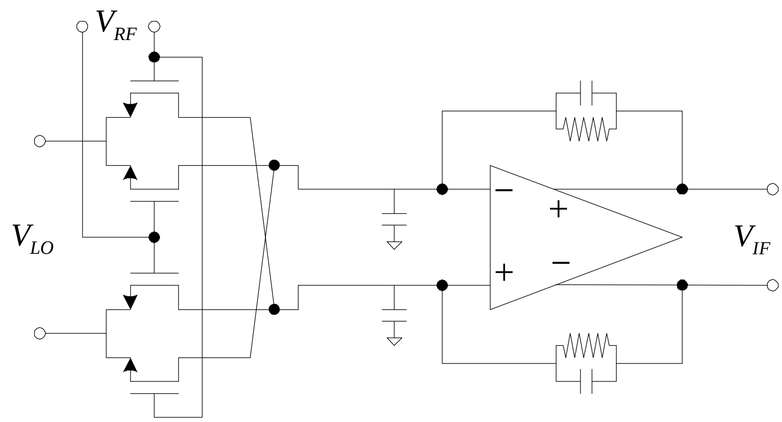

Figure 5.2: Potentiometric mixer circuit implementation.

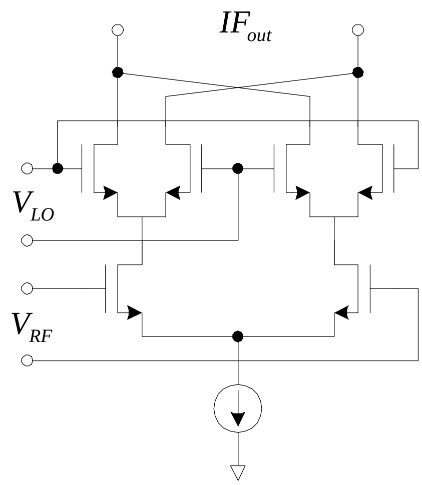

Figure 5.3: Gilbert type double balanced mixer

consumption due to LNA power requirement and a decrease in linearity because of the high-gain LNA's limitation.

The third mixer type in table 5.1, the Gilbert mixer as shown in figure 5.3, is used in many communication systems. This Gilbert type mixer performs a voltage to current conversion of the RF signal that can be modified by the LO signal. The advantage of this architecture is the conversion gain which occurs without adding much noise. This conversion gain of the mixer can be helpful if it is difficult to obtain

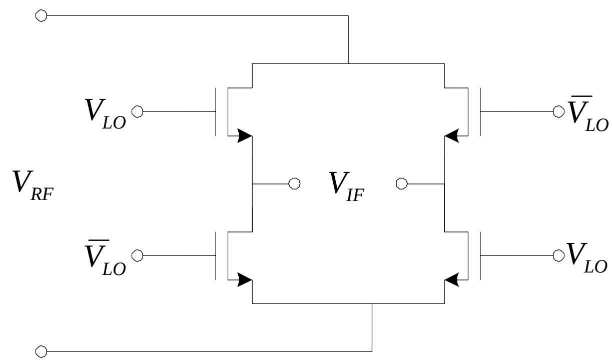

Figure 5.4: Voltage mixer circuit diagram

additional gain form the LNA block as is the case for the UWB LNA which has very wide-bandwidth. However because this Gilbert mixer uses a differential pair as its transconductance stage, this type of mixer is used in the narrow-bandwidth systems.

The last architecture in table 5.1 is the voltage mixer as illustrated in figure 5.4. This voltage mixer eliminates the voltage to current conversion of the RF signal and keeps signals in the voltage domain. Unlike the Gilbert type of mixer, the voltage mixer uses a capacitive load, which does not add noise to the system. As shown in table 5.1, compared with other types of mixers, this voltage mixer has the advantage for the low power consumption, low noise figure, and high linearity. However it has conversion loss. This is a significant disadvantage for the UWB system considered here because the UWB system it requires additional gain at the mixer.

Among the four architectures, the subsampling mixer and the potentiometric mixer can not be used for the UWB system because of their architectural disadvantages. The Gilbert type and the voltage mixer could be good candidates for the

UWB mixer but those two type of mixers also require major modifications to fit wide-bandwidth signal requirements.

5.1.2 Mixer for wide-bandwidth Signal

To design a mixer for a wide-bandwidth signal, the mixer must have broadband input characteristics, and high conversion gain to increase signal gain because the LNA, in a wide-bandwidth system, cannot provide enough gain with low power consumption. In addition to this requirement, usually the mixer requires differential input to reduce the mixer's noise figure and to increase linearity. To achieve differential signal for the UWB system, a wide-bandwidth balun may be required. However since the balun is usually designed with inductors [48], it is difficult to achieve broadband characteristics. Therefore as an alternative, there are a few active baluns, which have more freedom from the bandwidth constraints, that have been reported [40][18][20][39]. The major disadvantage of these active baluns is additional noise that they insert into the system.

To use a voltage mixer as a UWB mixer, the problems of conversion gain and differential RF input must be solved. To overcome the voltage mixer's loss, a multi-stage of a LNA block is required before the mixer. Then the cascaded multi-stage LNA block consumes a lot of power and chip area.

The Gilbert type mixer can give additional gain to the signal but still requires broadband characteristics and differential input. The easiest way to achieve

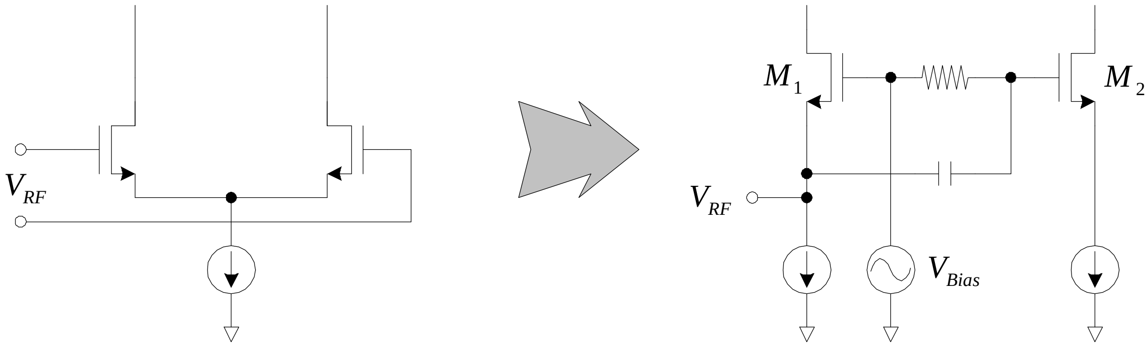

Figure 5.5: V-I conversion using the CS-CG pair.

the broadband characteristics is by using resistive termination at the input nodes [16][40]. However with this method, the resistor attached to the input increases the noise figure of the system.

Since the transconductance of the Gilbert mixer is used to transfer the input RF voltage to a current signal using the differential pair, it is possible using a pair of the common source(CS) and common gate(CG) amplifiers to generate a differential current signal as shown in figure 5.5. With this configuration, when both transistor M_1 and M_2 are the same size and working in the saturation region, the DC current of the CS-CG pair is the same because the V_{gs} of each transistor is same. Therefore the current of each current can be described as

$$I_{CS} = \frac{\beta}{2}(V_{bias} + V_{RF} - V_s - V_{th})^2 \tag{5.1}$$

$$I_{CG} = \frac{\beta}{2}(V_{bias} - V_{RF} - V_s - V_{th})^2 \tag{5.2}$$

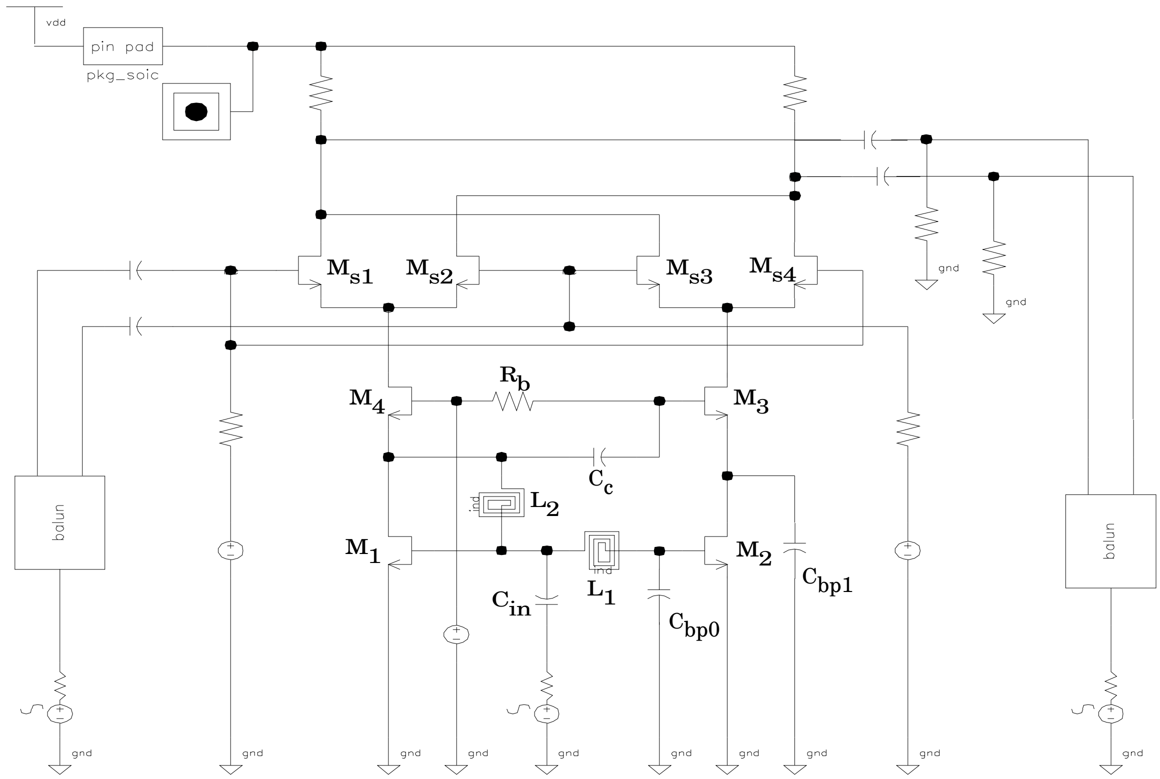

Figure 5.6: The wide-bandwidth mixer with CS-CG pair transconductance.

where $\beta = \mu_n C_{ox} W/L$. Therefore the drain current of each transistor in the CS-CG pair can be described as a function of differential input signals. With this configuration, the mixer acts like the double balanced mixer without using a balun. The other requirement of the broadband mixer, which is wide-bandwidth input characteristics, e.g., input impedance matching, can be satisfied with a few additional passive components.

Considering that there is a common gate configuration in the CS-CG pair, a $1/g_m$ termination can be applied to the system. The completed wide-bandwidth mixer with the CS-CG pair is illustrated in figure 5.6. In this figure, the transistor M_1 and

M_2 are connected as current mirrors to provide same DC current to each of the CS-CG transistors. The transistors M_3 and M_4 act as CS-CG pair. The L_1 and C_{bp0} are attached between the input and the transistor M_2 to block and bypass the undesired RF signal into the transistor M_2. The capacitance C_{bp1} bypasses the noise which is generated in transistor M_2. Therefore there are three AC ground connections at the drain and the gate of transistor M_2 and the DC biasing point at the gate of transistor M_4. The inductor L_2 is attached to make a $T-matching$ network in association with the input capacitance C_{in} and the AC blocking inductor L_1. This matching network ensures that the system maintains wide-bandwidth characteristics even if the g_m of the transistor M_4 becomes larger. The reason why we give g_m some freedom of sizing is that this g_m value and the mixer load directly affects the conversion gain. Suppose LO transistors, M_{s1}, M_{s2}, M_{s3} and M_{s4}, are perfect switches. Then the current flowing into the mixer load is [31]

$$\begin{aligned} I_{out} &= g_m \sin \omega_{RF} t \times (\frac{4}{\pi})(\sin \omega_{LO} t + \sin 3\omega_{LO} t + \ldots) \\ &\simeq (\frac{2}{\pi}) g_m \cos(\omega_{RF} - \omega_{LO}) t \end{aligned} \tag{5.3}$$

According to this equation, the mixer's voltage gain becomes

$$\text{Mixer Gain} = (\frac{2}{\pi}) \cdot g_m \cdot R_{load} \tag{5.4}$$

The designed wide-bandwidth mixer's input impedance characteristic is plotted in figure 5.7. This figure shows that the input impedance characteristic at the frequency of 0.8 GHz $\sim$ 1.6 GHz matched at 50 Ω. From this result, replacing the differential pair type V-I converter to the CS-CG pair, the Gilbert type mixer acts as double balanced mixer with only one input, and also it has wide-bandwidth input impedance matching with a few passive components. However to use this as a wide-bandwidth mixer, a few other broadband characteristics are required.

5.2 Mixer Analysis

In general, a mixer's quality can be specified by its conversion gain, noise figure, and linearity. In this section, these specifications are going to be evaluated for the designed wide-bandwidth mixer.

5.2.1 Conversion Gain of wide-bandwidth Mixer

A mixer's conversion capability can be illustrated in two different ways: power conversion gain and voltage conversion gain. Power conversion gain is defined to be the power delivered to the load divided by the power available from the source, as described in the previous chapter.

$$G_p = \frac{\text{power delivered to the load}}{\text{available power from the source}} \tag{5.5}$$

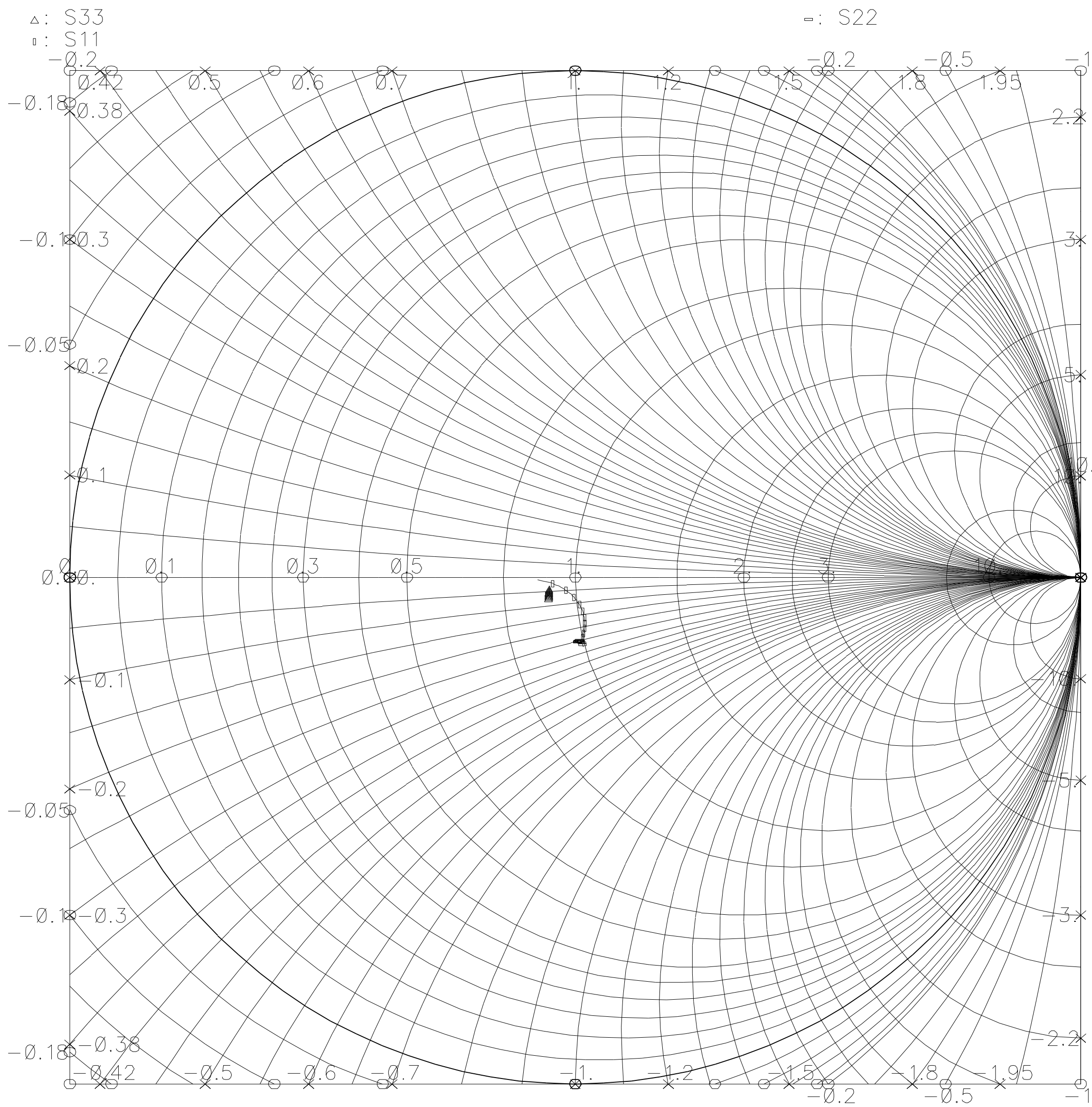

Figure 5.7: The input impedance matching of the wide-bandwidth mixer.

The voltage conversion gain, which is widely used as the mixer's conversion gain, is defined as the voltage amplitude across the output port divided by the source voltage amplitude.

$$G_v = \frac{\text{voltage amplitude across the output port}}{\text{source voltage amplitude}} \tag{5.6}$$

Therefore this definition can be described as

$$G_v = 20 \log \frac{A_{out}}{A_{RF}} \tag{5.7}$$

Usually a large conversion gain is desirable to minimize the system's noise figure because the large gain increases the system's signal strength. However excessive conversion gain may cause linearity degradation [45]. Figure 5.8 shows this mixer's conversion gain when different local oscillator signals are applied. The average conversion gain of this mixer is about 13 dB and the gain variation within desired frequency range is less than 0.5 dB. Compared to the conventional Gilbert type mixer shown in table 5.1, this modified type of mixer has more conversion gain and consumes only 6.6 mW of power.

5.2.2 Noise Consideration of the Mixer

Quantifying and accounting for a mixer's noise contribution is more complicated because its output response includes noise from across the input frequency band.

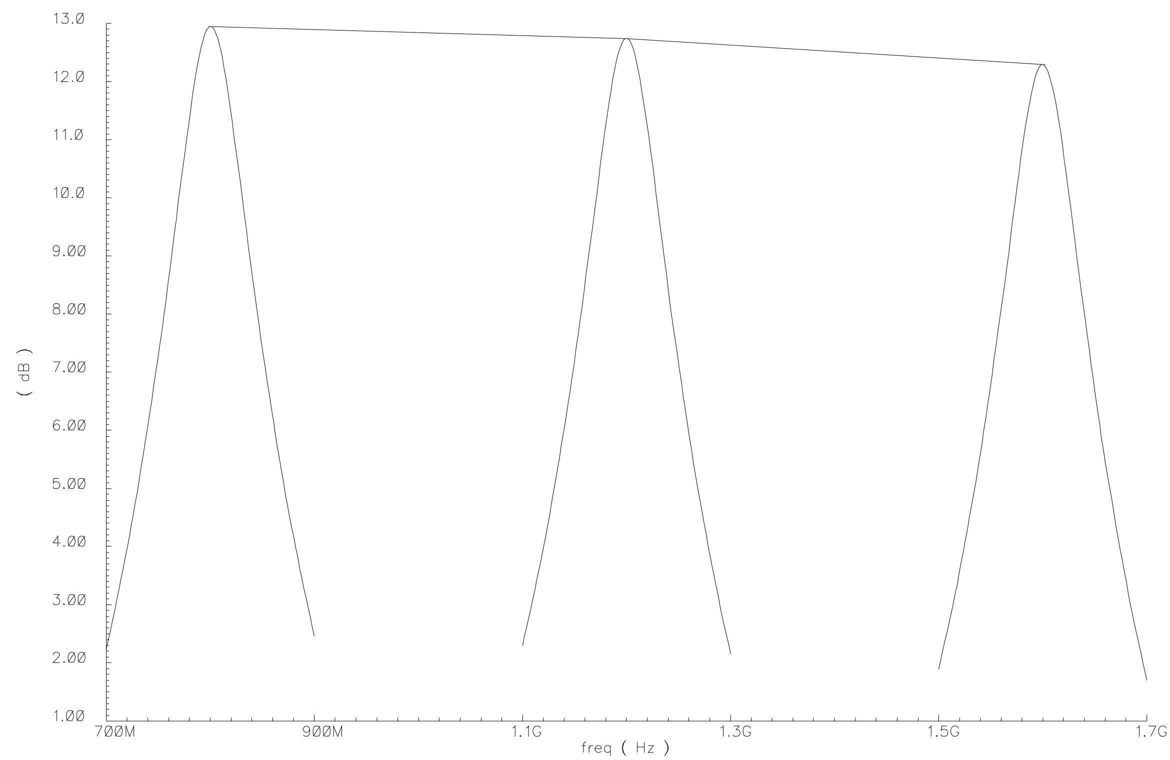

Figure 5.8: Mixer conversion gain when LO is 0.8 GHz, 1.2 GHz and 1.6 GHz

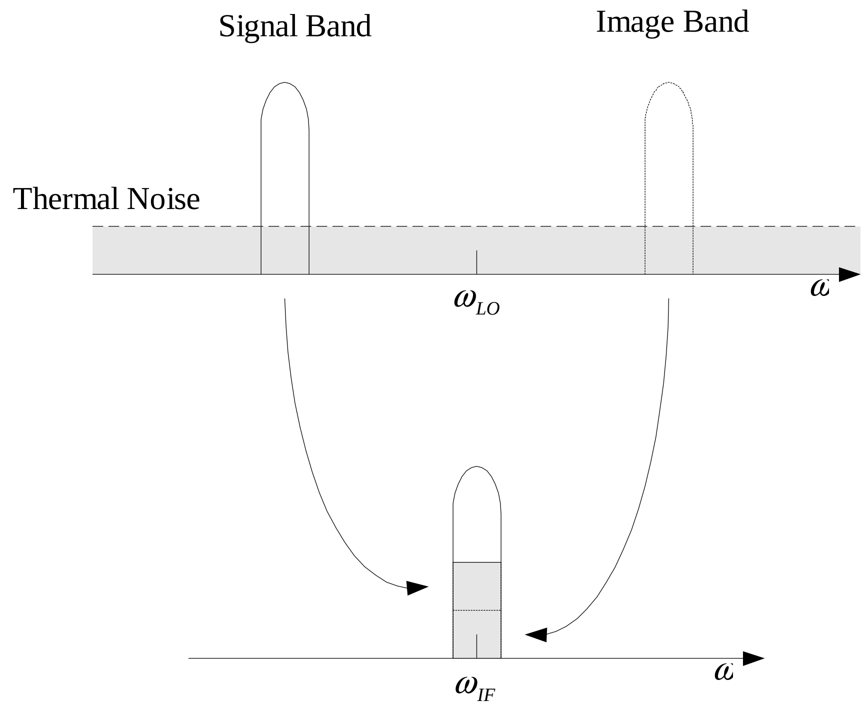

Figure 5.9: The single sideband noise by folding of the signal and image into the IF band

In many mixer noise analysis, two types of noise figures are used. One is the single sideband (SSB) noise figure and the other is the double sideband (DSB) noise figure. Figure 5.9 shows the down conversion process of narrow-bandwidth system. As shown in this figure, the noise in the signal band and the noise in the image band are translated to ω_{IF}. Therefore the output SNR becomes half of the input SNR if the frequency response of this mixer is same for the signal band and the noise band. This process provides the SSB noise figure of the mixer. The DSB noise figure can be described with figure 5.10. As shown in this figure, the input and output SNR is same. Therefore the noise figure of this mixer is 0 when the mixer

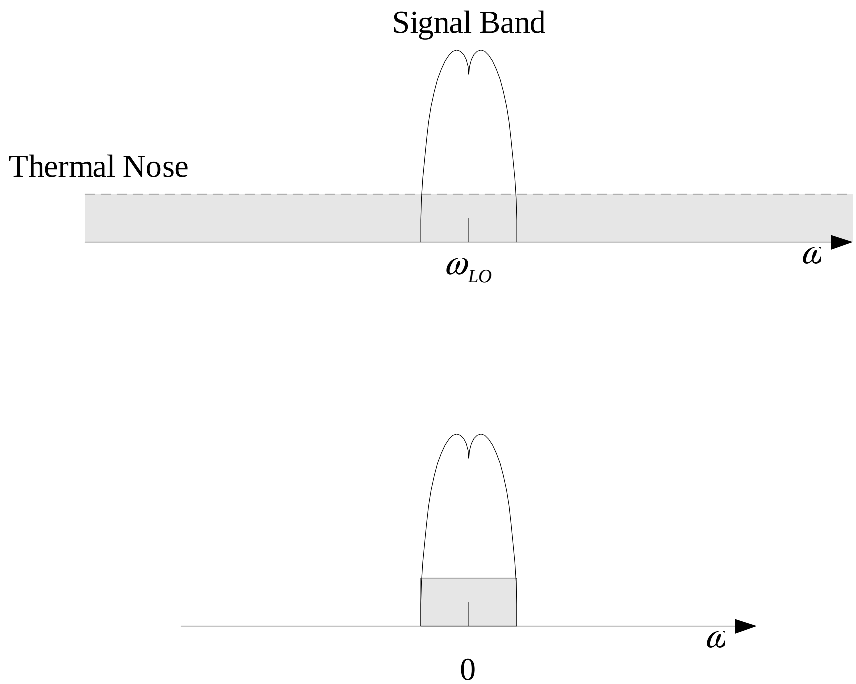

Figure 5.10: The double sideband noise

is ideal [29]. However these narrow-bandwidth noise analysis may not be applicable to the wide-bandwidth system because the template signal is not the same as a narrow-bandwidth local oscillator signal. Therefore to analyze the noise of the wide-bandwidth mixer, a more general approach to noise performance evaluation is necessary.

The noise sources in the mixer can be classified as low frequency noise and high frequency noise. In low frequency region, flicker noise (known as 1/f noise) is dominant and the high frequency region, the white noise is dominant. Considering that the UWB system uses a wide frequency range, both noise sources should be considered.

Basically an active mixer comprises three different part: an input transconductance, switches, and an output load. In the low frequency region, the noise in the transconductance is fed into switches and is translated into the frequency range of the incoming signal. Therefore the flicker noise at lower frequencies is upconverted to the LO frequency band. Another severe noise source in the low frequency region is the transistor switching noise which correlated with the flicker noise. This noise can be described as the spectrum of noise current at the mixer output[7].

$$\overline{i_{n,o}} = \frac{1}{\pi} \cdot \frac{I}{A} \cdot V_{nf} \tag{5.8}$$

where the I is the bias current, A is the amplitude of the LO signal, and V_{nf} is the flicker noise which feeds into the LO switch. From the equation 5.4, the current at the mixer output can be expressed as

$$I_o = \frac{2}{\pi} \cdot g_m \cdot V_{RF} \tag{5.9}$$

where the g_m is the input transistor's transconductance $g_m = I/(V_{GS} - V_th)$. Therefore the SNR which is related solely to the flicker noise at the LO switch can be

$$SNR_{nf} = \frac{2A}{(V_{GS} - V_th)} \cdot \frac{V_{RF}}{V_{nf}}. \tag{5.10}$$

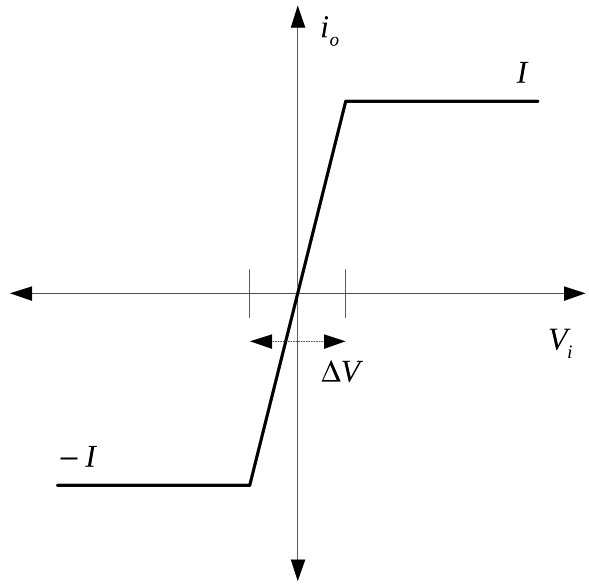

Figure 5.11: The I-V curve at the mixer switching pair.

This relationship shows that SNR improves by rasing the amplitude of LO, and by lowering the transconductance over-drive.

In the high frequency region, the major noise source is the thermal noise. Therefore from transistor noise analysis, when the input noise is white and stationary, then its power spectral density is

$$\overline{V_n^2} = \frac{4kT\gamma}{g_m} \tag{5.11}$$

where γ is the channel noise factor, traditionally 2/3 for a long channel device and much higher for a short channel device, and g_m is the transconductance of the switch at zero-crossing as shown in figure 5.11. From this figure, the transconductance can be described as

$$g_m = \frac{2I}{\Delta V} \tag{5.12}$$

To find out the output current noise due to the single switching transistor, from equations 5.11 and 5.12,

$$\begin{aligned} \overline{i_{n,o}^2} &= \overline{V_n^2} \cdot g_m^2 \\ &= 4kT\gamma \frac{2I}{\Delta V}. \end{aligned} \tag{5.13}$$

The ΔV can be described as the product of the slope and the period of the injected LO signal. Suppose the LO signal is sine wave, $V_{id} = 2A \sin(\omega_{LO} t)$, then, at $t = 0$, the slope of the LO signal is $S = 2A\omega_{LO}$. And the period of the LO is simply calculated as $T = 2\pi/\omega_{LO}$. Therefore the output noise current density of the switch is

$$\overline{i_{n,o}^2} = 4kT\gamma \frac{I}{\pi A} \tag{5.14}$$

where A is the amplitude of the LO and I is the bias current. As seen in this equation, the output noise of the switches is a function of the bias current and the amplitude of the LO signal.

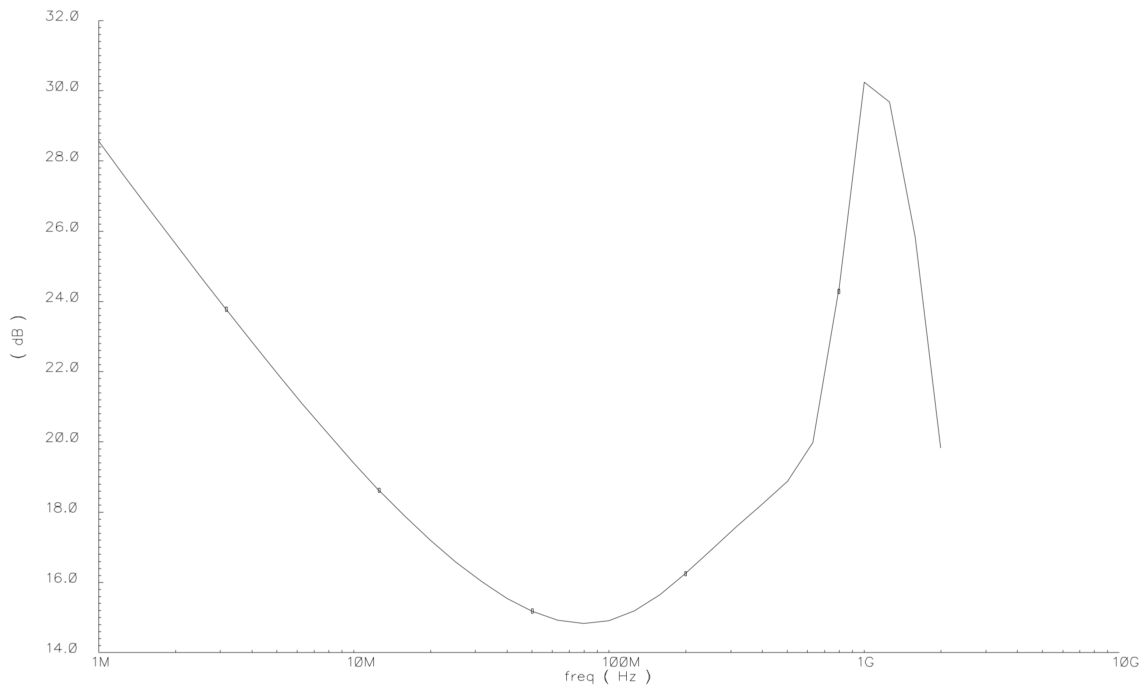

Figure 5.12: Noise figure deduced from output noise spectrum

To determine the noise figure of the designed mixer, the periodic noise (PNoise) analysis in the SPECTRE-RF software is used [2][38]. This analysis is similar to the noise analysis which previously was described, except that it includes frequency conversion effects. PNoise is a two step process. In the first step, periodic steady state analysis is used to compute the response to a large periodic signal. In the second step, the resulting noise performance is computed. With this PNoise analysis, bias dependent noise sources and the transfer function from the noise source to the output are considered in computing the total output noise.

With the SPECTRE-RF PNoise analysis, the noise figure of the designed mixer is plotted in figure 5.12. As shown in this figure, the mixer's noise figure is about 15 dB.

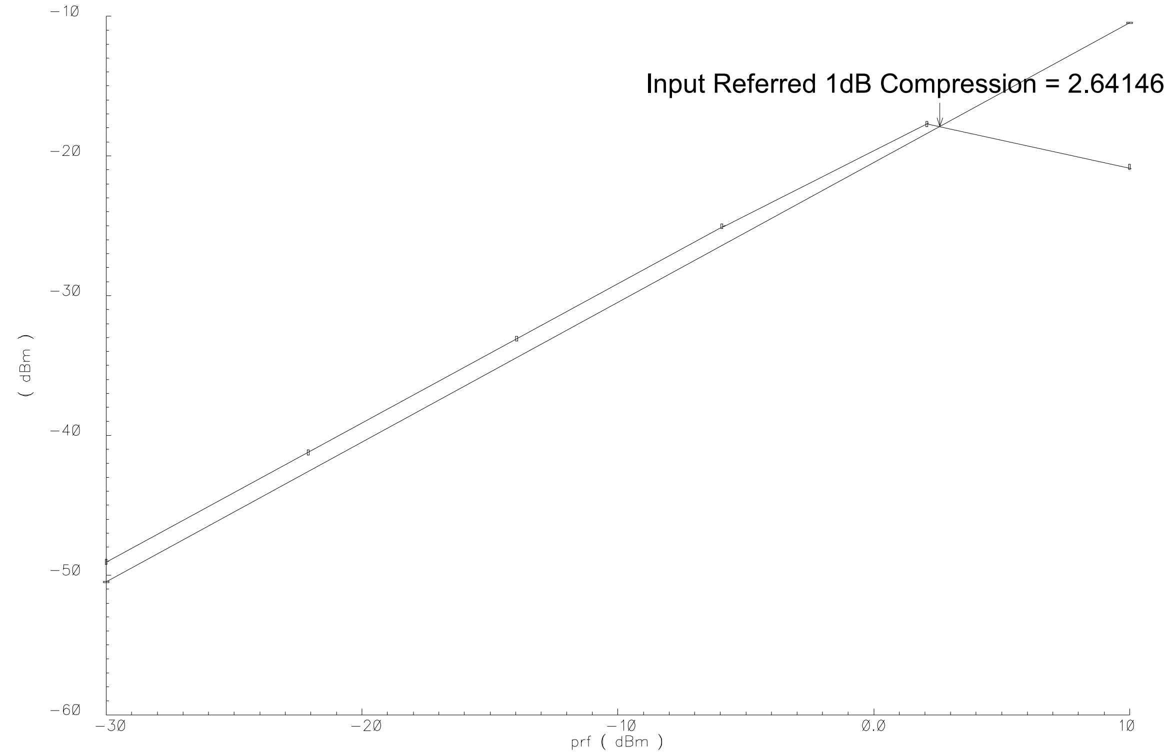

Figure 5.13: 1 dB compression point of the mixer when 0.8 GHz input signal is applied.

5.2.3 Linearity

In the UWB mixer, losing linearity distorts the signal. Like the amplifier, if the conversion gain becomes too large, the mixer's linearity will suffer and its dynamic range reduced. Since the UWB signal is composed of short pulses, the incoming signal power for short periods of time is large. Therefore the dynamic range of this mixer should be large enough to cover the power of the incoming signal. The 1 dB compression points of the UWB mixer are plotted in figures 5.13, 5.14, and 5.15. These figures are plotted for three frequencies within the frequency range applied to the mixer. As shown in these figures, the 1 dB compression point is

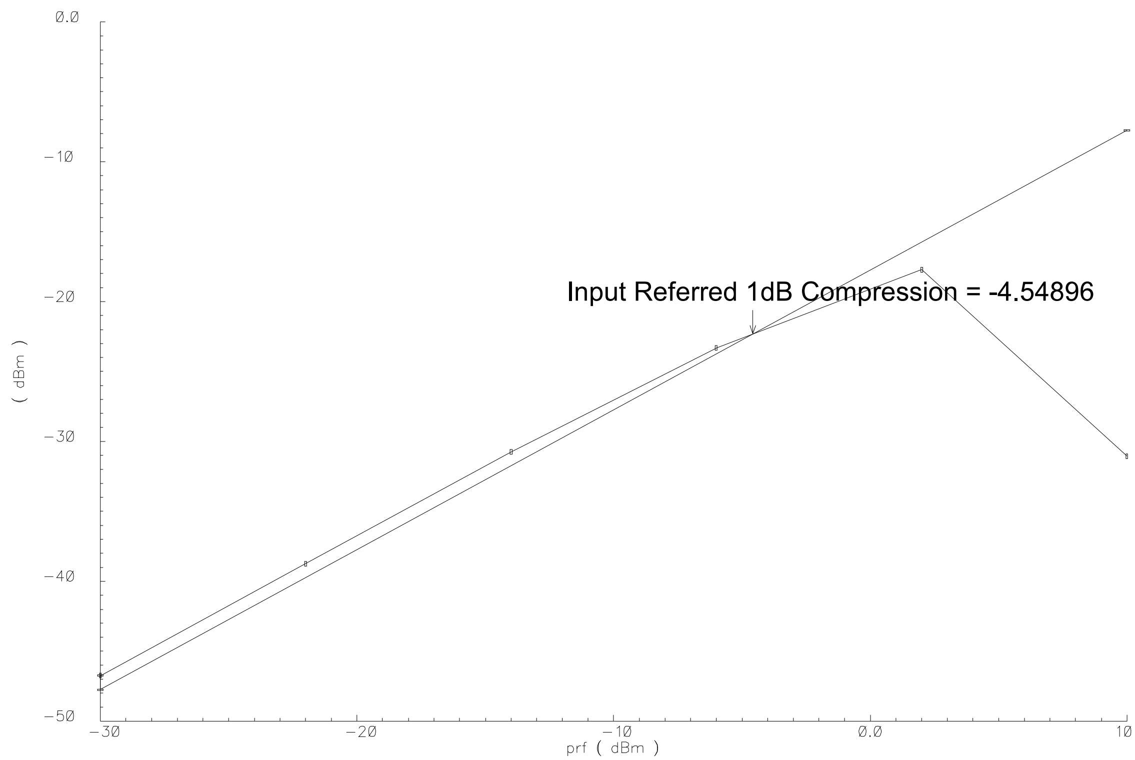

Figure 5.14: 1 dB compression point of the mixer when 1.2 GHz input signal is applied.

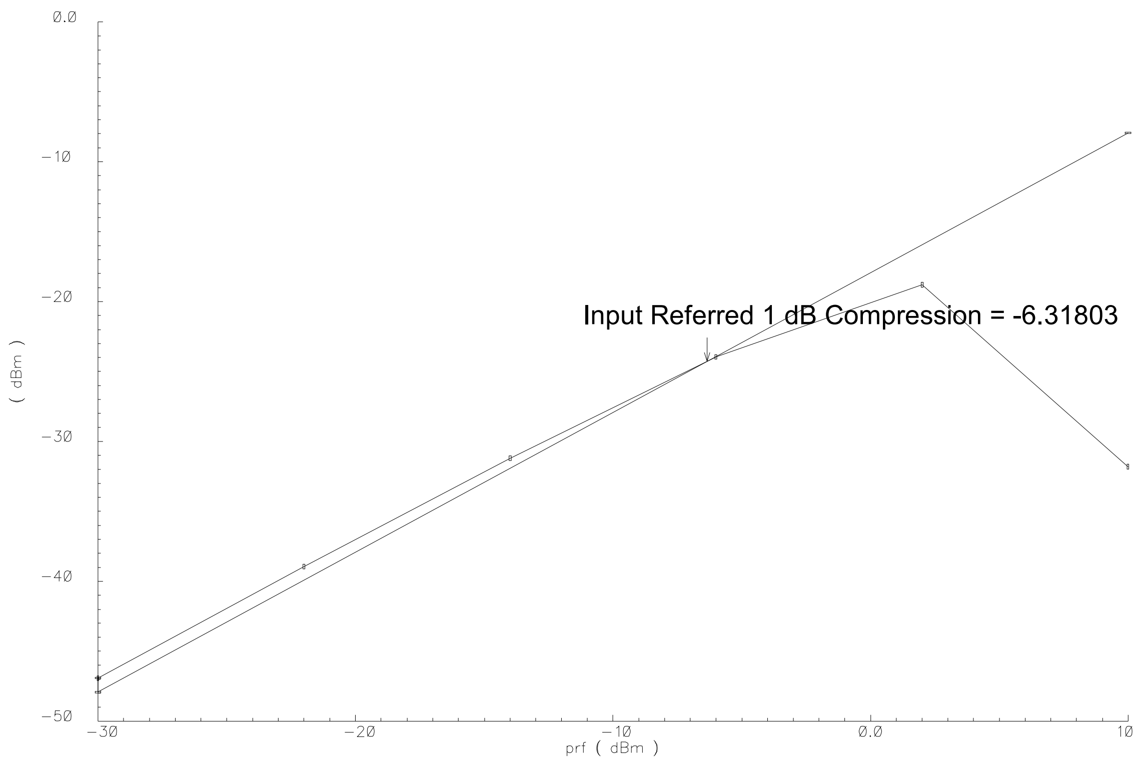

Figure 5.15: 1 dB compression point of the mixer when 1.6 GHz input signal is applied.

Table 5.2: The designed Mixer performance summary

Conversion gain	NF	P_{1dB}	Power consumption
13±0.5 dB	about 15 dB	-6.3 dBm	6.6 mW

slightly degraded as the frequency increases. This effect is usually caused by the large switching transistor's gate area or by lowering V_{GS} of the switching transistor.

In the wide-bandwidth system, the lowest 1 dB compression point (P_{1dB}) in the UWB frequency range should be selected as its dynamic range. Therefore the worst 1 dB compression point of the interest frequency range is -6.3 dBm.

5.3 Summary of the UWB Mixer

The UWB mixer has been designed and analyzed. The table 5.2 shows the system specification of this mixer. In this mixer, a new input transconductance stage has been introduced. This new type of input stage makes double balanced mixer characteristics available with only a single input. Therefore this mixer eliminates the balun which has been used at the front-end of many RF systems. Also this type of mixer gives very good input impedance matching, even for a wide-bandwidth system using a few passive components, while improving the mixer conversion gain.

Chapter 6

Contribution and Conclusion

In this dissertation, two major tasks have been explored. One is the construction of new correlator template generation architecture of the ultra wide bandwidth system. The other is the design of the front-end components of this system. As a conclusion to this dissertation, the key contributions presented in previous chapters are summarized.

6.1 Summary

A new type of the UWB system has been introduced in the previous chapters. This system uses a sinusoidal template in the correlator instead of the second derivative Gaussian model template. The sinusoidal template is simple to implement with current technology. Also it reduces system complexity without degrading the system performance significantly compared to the ideal system. Since the basic architecture of this system comes from the analog phase locked loop, this system also has a simple clock locking mechanism for synchronization.

The low noise amplifier and mixer of this ultra wide bandwidth system have been designed. Although the new UWB system uses conventional parts which can be implemented with current technology, the key components at the front-end are different from current technologies. The major differences of these components from the current RF devices is that they possess the wide bandwidth characteristics as described in previous chapters.

For the LNA, this wide bandwidth characteristic has been achieved by employing a shunt-series feedback topology. To overcome the high power consumption problem, optimal biasing has been applied to this topology. Also the frequency compensated matching technique has been applied to increase its gain flatness.

The UWB mixer is designed in a new way. The common source-common gate pair replaces the transconductance part of the conventional Gilbert type mixer. This approach makes available double balanced mixer characteristics with only a single input. Since this mixer requires only one input, no balun is necessary. The main advantage of this architecture is its wide bandwidth characteristic, which is our primary goal.

6.2 Recommended for Future Work

There are a few issues that await exploration in future studies. Since the ultra wide bandwidth system is new in the communication field, research is still required in many areas. In particular, a proven noise model for the wide bandwidth system is required. Since most analytical methods for communication devices are developed for narrow bandwidth systems, a new noise analysis method is necessary for the wide bandwidth system.

Reference List

[1] R. Benton, Nijjar M, C.Woo, A. Podell, G Horvath, E. Wilson, and S. Mitchell. GaAs MMICs for an integrated GPS front-end. In *GaAs-IC Symposium Digest of Technical Reports*, pages 123–126, 1992.

[2] Cadence Design Systems, Inc. *Affirma RF Simulator (SpectreRF) User Guide*, 1999.

[3] J.Y.C. Chang, A.A. Abidi, and M. Gaitan. Large suspended inductors on silicon and their use in a 2 μm CMOS RF amplifier. *IEEE Journal of Solid-State Circuits*, 14(5):246–248, May 1993.

[4] Leon W. Couch. *Digital and Anlog Communication Systems*. Prentice Hall, 2001.

[5] D. C. Cox. Wireless personal communications: What is it? *IEEE Personal Communications*, 2(2):20–35, April 1995.

[6] Jan Crols and Michel S. J. Steyaert. A 1.5 GHz highly linear CMOS downconversion mixer. *IEEE Journal of Solid-State Circuits*, 30(7):736–742, July 1995.

[7] Hooman Darabi and Asad A. Abidi. Noise in RF-CMOS mixers: A simple physical model. *IEEE Transactions on Solid State Circuits*, 35(1):15–25, January 2000.

[8] Christian C. Enz and Yuhua Cheng. MOS transistor modeling for RF IC design. *IEEE Transactions on Solid State Circuits*, 35(2):186–201, February 2000.

[9] Qiuting Huang, Francesco Piazza, Paolo Orsatti, and Tatsuya Ohguro. The impact of scaling down to deep submicron on CMOS RF circuits. *IEEE Journal of Solid State Circuits*, 33(7):1023–1036, July1998.

[10] Ed. James D. Taylor. *Introduction to Ultra-Wideband Radar Systems*. CRC Press, 1995.

[11] Johan Janssens, Jan Crols, and Michiel Steyaert. A 10 mW inductorless, broadband CMOS low noise amplifier for 900 MHz wireless communications. In *Custom Integrated Circuits Conference*, pages 75–78, 1998.

[12] Andrew N. Karanicolas. A 2.7 v 900 MHz CMOS LNA and mixer. *IEEE Journal of Solid-State Circuits*, 31(12):1939–1944, December 1996.

[13] Cheon Soo Kim, Hyun Kyu Yu, Hanjin Cho, Seonghearn Lee, and Kee Soo Nam. CMOS layout and bias optimization for RF IC design applications. In *IEEE MTT-S Digest*, pages 945–948, 1997.

[14] Beom Kyu Ko and Kwyro Lee. A new simulation noise and input power matching technique for monolitic LNA's using cascode feedback. *IEEE Transactions on Microwave Theory and Techniques*, 45(9):1627–1630, September 1997.

[15] K. W. Kobayashi, R. Esfandiri, A. K. Oki, D. K. Umemoto, J. B. Camou, and M. E. Kim. GaAs heterojuction bipolar transistor MMIC DC to 10 GHz direct-coupled feedback amplifier. In *GaAs IC Symposium*, pages 87–90, 1989.

[16] Kevin W. Kobayashi, Ryan Desrosiers, Augusto Gutierrez-Aitken, John C. Cowles, Benjamin Tang, L. T. Tran, Thomas Ray Block, Aaron K. Oki, and Dwight C. Streit. A DC - 20 GHz InP HBT balanced analog multiplier for high data rate direct digital modulation and fiber optic receiver application. *IEEE Transactions on Microwave Theory and Techniques*, 48(2):194–202, February 2000.

[17] Kevin W. Kobayashi and Aaron K. Oki. A low noise baseband 5 GHz direct coupled HBT amplifier with common base active input match. *IEEE Micrwave and Guided Wave Letters*, 4(11):373–375, November 1994.

[18] Haruhiko Koizumi, Shunsuke Nagata, Kazuki Tateoka, Kunihiko Kanazawa, and Daisuke Ueda. A GaAs single balanced MMIC with built in active balun for personal commnication system. In *Microwave and Milimeter Wave Monolitic Circuits Symposium*, pages 77–80, 1995.

[19] Haruhiko Koizumi, Atsushi Noma, Tsuyoshi Tanaka, Kunihiko Kanazawa, and Daisuke Ueda. A GaAs MMIC chip set for mobil communications using on ship ferroelectric capacitors. *IEEE Journal of Solid State Circuits*, 31(6):835–839, June 1996.

[20] Chang-Seok Lee, Min-Gun Kim, Jae-Jin Lee, Kwang-Eui Pyun, and Hyung-Moo Park. A low noise amplifier for a multi-band multi-mode handset. In *IEEE Radio Frequency Integrated Circuits Symposium*, pages 47–50, 1998.

[21] Kyeongho Lee, Joonbae Park, Jeong-Woo Lee, Seung Wook Lee, Hyoung-Ki Huh, Deog-Kyoon Jeong, and Wonchan Kim. A single chip 2.4 GHz direct conversion CMOS receiver for wireless local loop using one third frequency local oscillator. In *Symposium on VLSI Circuits Digest of Technical Papers*, pages 42–45, 2000.

[22] Thomas H. Lee. *The Design of CMOS Radio-Frequency Integrated Circuits*. Cambridge, Cambridge, 1998.

[23] W. C. Y. Lee. Applying the intelligent cell concept to PCS. *IEEE Transactions on Vehicular Technology*, 43(3):638–643, Aug 1994.

[24] Reinhold Ludwig and Pavel Bretchko. *RF Circuit Design*. Prentice Hall, 2000.

[25] M. A. Luqueze, D. Consonni, and C. Y. Yamada. MMIC wideband low noise amplifier. In *SBMO/IEEE MTT-S IMOC '99 Proceedings*, pages 264–266, 1999.

[26] Tajinder Manku, Galen Beck, and Etty J. Shin. A low-voltage design technique for RF integrated circuits. *IEEE Transactions on Circuits and Systems-II*, 45(10):1408–1413, October1998.

[27] Robert G. Meyer and William D. Mack. A 1 GHz BiCMOS RF front-end IC. *IEEE Journal of Solid-State Circuits*, 29(3):350–355, March 1994.

[28] Vijay Nair, Saied Tehrani, Rimantas L. Vaitkus, and Douglas G. Scheitlin. Low power HFET down converter MMIC's for wireless communication applications. *IEEE Transactions on Microwave Theory and Techniques*, 43(12):3043–3047, December 1995.

[29] Behzad Razavi. *RF Microelectronics*. Prentice Hall, Upper Saddle River NJ, 1998.

[30] Ahmadreza Rofougaran, James Y.C. Chang, Maryam Roufougaran, and Asad A. Abidi. A 1 GHz CMOS RF front-end IC for a direct conversion wireless receiver. *IEEE Journal of Solid-State Circuits*, 31(7):880–889, July 1996.

[31] Jacques C. Rudell, Jia-Jiunn Ou, Thomas Byunghak Cho, George Chien, Francesco Brianti, and Jeffrey A. Weldon. A 1.9-GHz wide-band if double conversion CMOS receiver for cordless telephone application. *IEEE Journal of Solid-State Circuits*, 32(12):2071–2088, December 1997.

[32] R.A. Scholtz. Multiple access with time-hopping impulse modulation. In *Proc. Military Comm. conf.*, pages 11–14, October 1993.

[33] Derek K. Shaeffer and Thomas H. Lee. A 1.5-v, 1.5-GHz CMOS low noise amplifier. *IEEE Journal of Solid State Circuits*, 32(5):745–759, May1997.

[34] Arvin R. Shahani, Derek K. Shaeffer, and Thomas H. Lee. A 12-mA wide dynamic range CMOS front-end for a portable GPS receiver. *IEEE Journal of Solid-State Circuits*, 32(12):2061–2070, December 1997.

[35] David H. Shen, Chien-Meen Hwang, Bruce Lusignan, and Bruce A. Woodey. A 900 MHz RF front-end with integrated discrete-time filtering. *IEEE Journal of Solid-State Circuits*, 31(12):1945–1954, December 1996.

[36] Mitsuru Shinagawa, Yukio Akazawa, and Tsutomu Wakimoto. Jitter analysis of high speed sampling systems. *IEEE Journal of Solid State Circuits*, 25(1):220–224, February 1990.

[37] Suharli Tedja, Jan Van der Spiegel, and Hugh H. Williams. Analytical and experimental studies of thermal noise in MOSFET's. *IEEE Transactions on Electron Devices*, 41(11):2069–2075, November 1994.

[38] Ricardo Telichevesky and Ken Kundert. Receiver characterization using periodic small signal analysis. In *Custom Integrated Circuits Conference*, pages 449–452, 1996.

[39] King Chun Tsai and Paul R. Gray. A 1.9 GHz, 1 w CMOS class-e power amplifier for wireless communications. *IEEE Journal of Solid State Circuits*, 34(7):962–970, July 1999.

[40] M.C. Tsai, M.J. Schindler, W. Struble, M. Ventresca, R. Binder, R. Waterman, and D. Danzilio. A compat wideband balanced mixer. In *IEEE MTT-S Digest*, pages 5–7, 1994.

[41] Y. Tsividis. *Operation and Modeling of the MOS Transistor*. McGraw Hill, Boston, second edition, 1999.

[42] Bing Wang, James R. Hellums, and Charles G. Sodini. MOSFET termal noise modeling for analog integrated circuits. *IEEE Journal of Solid State Circuits*, 29(7):833–835, July 1994.

[43] M.Z. Win, R.A. Scholtz, and L.W. Fullerton. Time-hopping SSMA techiques for impulse radio with an analog modulated data subcarrier. In *Proceedings of IEEE Fourth International Symposium on Spread Spectrum Techniques and Applications*, pages 359–364, Mainz, Germany, September 1996.

[44] Paul Withington. Impulse radio overview. Technical report, Time Domain Co., 1998.

[45] Stephen Wu and Behzad Razavi. A 900-MHz/1.8-GHz CMOS receiver for dual-band applications. *IEEE Journal of Solid State Circuits*, 33(12):2178–2185, December1998.

[46] Jiansheng Xu, Yisong Dai, and Li Yaqen. The study of the relation between $r_n - g_n$ noise model and $e_n - i_n$ noise model of an amplifier. *IEEE Transactions on Circuits and Systems-I:Fundamental Theory and Applications*, 45(2):154–156, February 1998.

[47] Kazuya Yamamoto, Takao Moriwaki, Takayuki Fujii, Jun Otsuji, Miyo Miyashita, Yukio Miyazaki, and Kazuo Nishitani. A 2.2 v operation, 2.4 GHz single chip GaAs MMIC tranceiver for wireless applications. *IEEE Journal of Solid State Circuits*, 34(4):502–512, April 1999.

[48] Jianjun J. Zhou and David J. Allstot. Monolitic transformers and thier application in a differential CMOS RF low-noise amplifier. *IEEE Journal of Solid State Circuits*, 33(12):2020–2027, December1998.